2003

Quiet wind tunnel design

Christopher John Vincent
Lehigh University

Vincent, Christopher John

Quiet Wind Tunnel Design

May 2003

QUIET WIND TUNNEL DESIGN

By

Christopher John Vincent

A Thesis

Presented to the Graduate and Research Committee

of Lehigh University

in Candidacy for the Degree of

Master of Science in

In

Mechanical Engineering

Lehigh University

May 2003

CERTIFICATE OF APPROVAL

This thesis is accepted and approved in partial fulfillment of the requirements for the degree of Master of Science in The Department of Mechanical Engineering and Mechanics.

03/18/03

Date

Professor Donald Rockwell
Thesis Advisor

Professor Herman Nied
Department Chair

TABLE OF CONTENTS

LIST OF FIGURES

ABSTRACT

This thesis presents the design of an experimental testing facility that will be used to study flow-acoustic coupling. Flow-acoustic coupling is the condition where flow and acoustic characteristics mutually influence one another. The aim of the present design work is construction of a wind tunnel that is void of acoustic influence, so that the fluid dynamic contribution to flow-acoustic coupling can be isolated. Anticipation of flow-acoustic behavior is based on prior studies of both coupled and isolated flow and acoustic behavior. The quiet tunnel layout is based on one of two concepts that resemble existing tunnels described in the literature. The elected concept is based on its potential to accommodate acoustics, fluid mechanics, instrumentation, and structural requirements for the desired facility. Techniques of assessing these requirements and justification for the final wind tunnel design are presented in this work.

1 INTRODUCTION

The focus of this thesis is on design considerations for an experimental facility that will be used in studying flow-acoustic coupling of a side branch cavity flow system. The facility will be a new addition to the Fluid Mechanics Research Laboratories at Lehigh University. There are instances similar to the subject facility presently in existence, but published literature that addresses how to design such a facility could not be found. The following sections provide background information for the design arguments. An overview of flow-acoustic coupling and quantitative assessment techniques is presented in Section 1 along with descriptions of similar, existing facilities, as well as, specific project goals including the incentive for conducting research on flow-acoustic coupling.

1.1 Motivation

Flow-induced vibration is a problem that hinders both internal and external flow systems. It is caused by the unsteady loading of flow boundaries from periodic vortex-body interaction, periodic acoustical perturbations, or a combination of both. Flow-acoustic coupling is a phenomenon where vortex-body interactions and acoustical perturbations mutually influence one another to occur regularly, with the same frequency.

The coupled effect of this self-excitation can produce vibration amplitudes that are much larger than either of the individual contributions.

Flow-acoustic coupling is most commonly found to occur in internal flow systems that possess discontinuous changes in cross-section and high flow rates. It is a problem of particular concern to designers of power generation systems. By itself, the coupled effect of periodic vortex-body interaction and acoustic disturbance can be sufficient to cause fatigue, yielding, or fracture failure of flow containers or their supporting structures. But, when resonance caused by flow-acoustic coupling is coincident with a resonant frequency of either the flow container or supporting structure, system failure may be inevitable; especially if flow-acoustic coupling was never considered in the system design. Losses associated with such a failure may be substantial should it cause a power plant to go off-line or disable the propulsion system in a Navy vessel.

The aim of researching flow-acoustic coupling is to reveal the mechanics of the phenomenon so that it may be addressed in the design phase of high energy flow systems where the risk of losses is minimal. Until recently, measuring instrument limitations have forced experimental analysis of flow-acoustic coupling to be performed with independent studies. Vortex-body interaction was usually studied in a flow system equipped with instrumentation for flow visualization that was kinematically similar to the system that initiated the research. Acoustical disturbances were usually modeled with free surface experiments using shallow water channels. Free surface waves were held analogous to their compressive counterparts.

Now, with the availability of high speed, high density particle imaging systems, to measure flow velocity fields, and high sensitivity, high resolution pressure transducers, to measure the unsteady static pressure in those fields, acoustically coupled flow systems may be precisely modeled in the laboratory. These measurement tools can fully characterize the flow field, not only while the system is resonating, but during transient conditions as well.

1.2 Research Objective

The objective for the following work is to present design considerations made in developing an experimental facility that can accommodate quantitative examination of flow-acoustic coupling occurring in cavity flow. Of particular interest are threshold velocities for incipient coupling, frequency and magnitude specifications for dominant modes, and the variation of these parameters with cavity depth and boundary layer thickness at separation (Rockwell, 2000). The project was stimulated by complications occurring in an air flow system possessing a deep side branch cavity and the success other researchers have had studying similar flows in quiet (free of acoustical perturbations) wind tunnels. While the project outlined here required construction of the experimental facility, the presented work only addresses design considerations that were made in preparation for construction.

1.3 Flow-Acoustic Coupling

Studies of the fluid dynamic contribution to flow-acoustic coupling, as it pertains to systems possessing cavity flow, have been performed in isolation from acoustical influence by Rockwell and Naudascher (1978, 1979) and by Knisely and Rockwell (1982). These studies reveal flow physics that cause periodic variations of static pressure on bounding walls, near the mouth of a shallow cavity. The studies show that the variations are caused by vortex formation and translation within the shear layer at the cavity mouth and impingement of the propagating vortex on the downstream cavity corner. Figures 1 & 2 illustrate this behavior using qualitative visualization techniques.

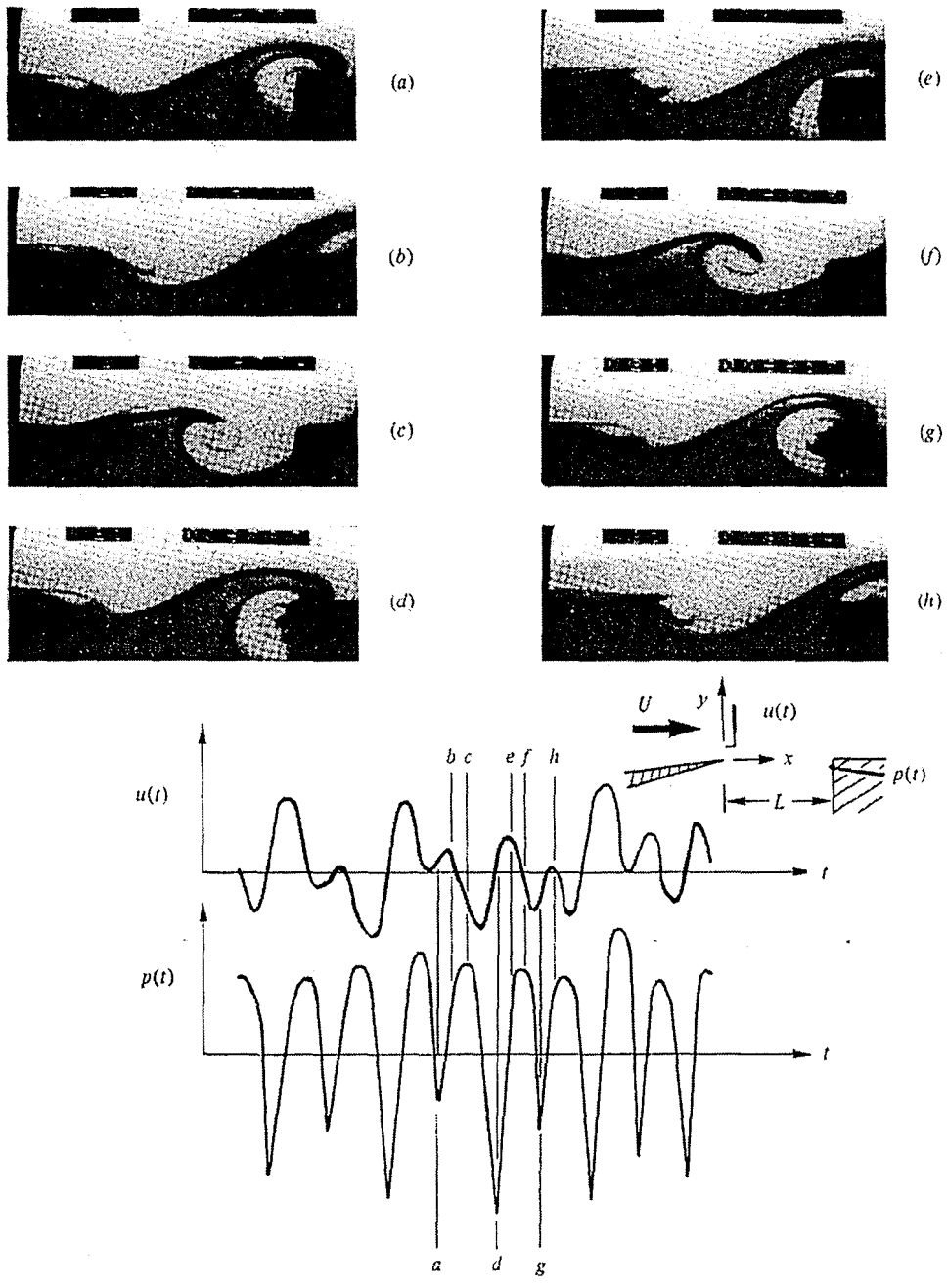

Figure 1 – Visualization of fluid dynamics that occur in cavity flow in absence of acoustical influence accompanied by corresponding velocity and pressure measurements. (Rockwell & Knisely, 1982)

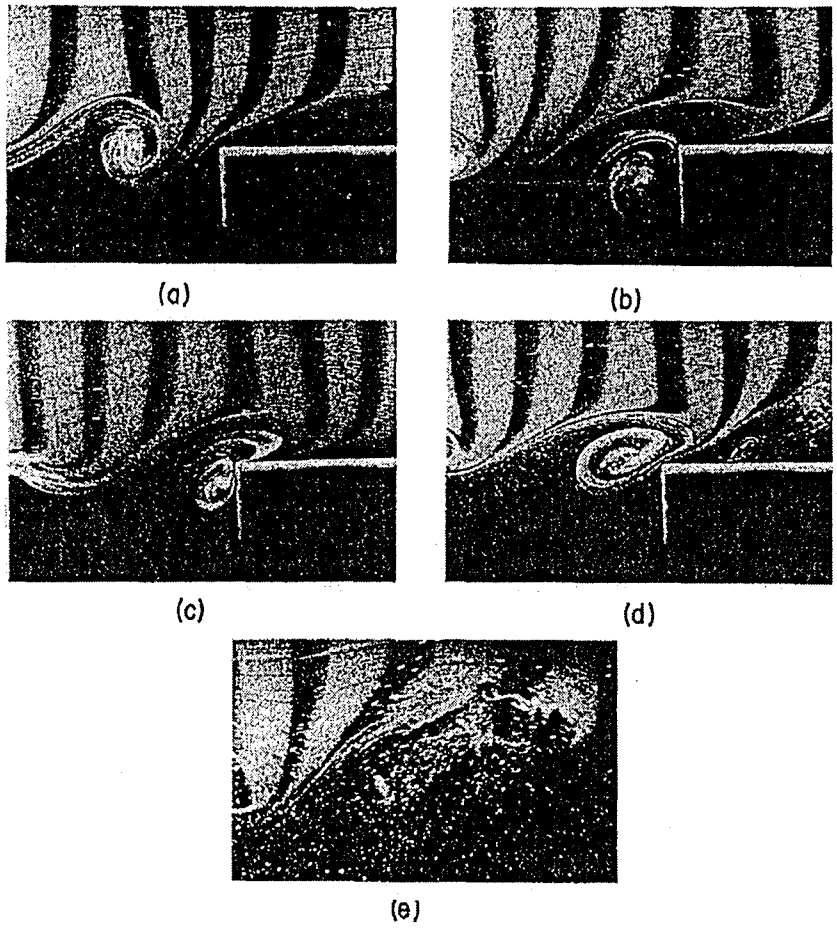

Figure 2 – Hydrogen bubble visualization of: (a) typical vortex approaching impingement edge of cavity; (b) complete clipping of vortex; (c) partial clipping of vortex; and (d) escape of vortex. Also shown is the same flow in absence of the downstream cavity corner (e). (Rockwell & Knisely, 1978)

An experimental result presented in all of these studies that is significant to the present investigation, is that the frequency of the pressure oscillations caused by the periodic vortex-body interaction may be predicted by non-dimensional analysis. Empirical data presented in these studies shows that the frequency of pressure oscillations occurring at the mouth of the cavity may be determined with the non-dimensional

Strouhal number, S_n, approximately equal to 0.5, 1.0, and 1.5 for the first three modes of resonance. That is:

$$S_n = \frac{f_n L}{U} \approx 0.5,\ 1.0, \text{ and } 1.5 \text{ for modes } 1,\ 2, \text{ and } 3, \text{ respectively } (\ 1 < L/W < 6\ ) \qquad (1)$$

This result is presented graphically in Figures 3. Figure 4 confirms that mode 2 resonance was more likely to occur in pressure spectrum data for various combinations of flow velocity and cavity geometry used in these studies.

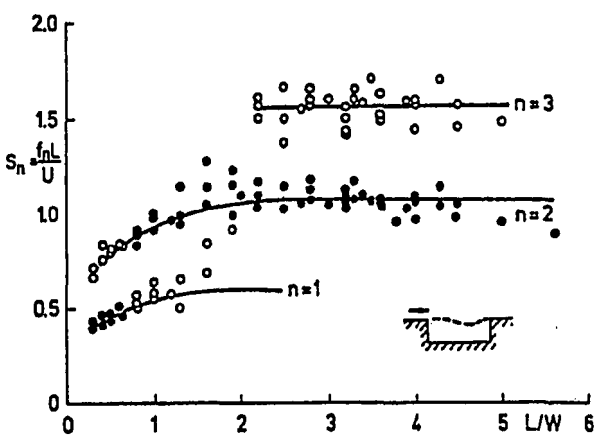

Figure 3 – Variation of non-dimensional oscillation frequency (Strouhal number) with cavity geometry. (Rockwell & Naudascher, 1978)

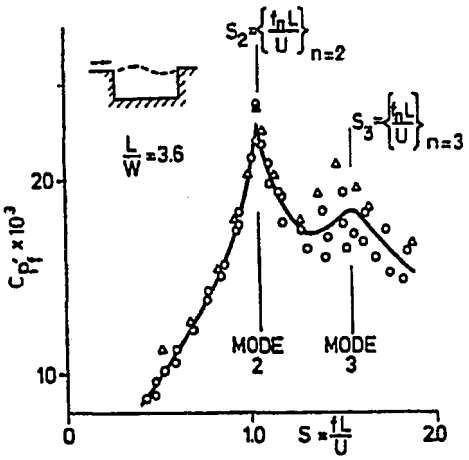

Figure 4 – Variation of pressure coefficient with Strouhal number. (Rockwell & Naudascher,1978)

While this functional relationship has been proven to be valid for *shallow* cavities with length, L, to depth, W, ratios ranging from 1 to 6, it is assumed to be applicable to the side branch cavity ($L/W < 1$) that is being considered here. The domain of $L/W < 1$

was not considered in the aforementioned studies because it is unclear whether acoustical disturbances, propagating along the depth of the cavity, are introduced. However, in the absence of such disturbances, vortex formation, translation, and impingement within the cavity shear layer are not dependent on the depth of static fluid that exists in the cavity. Therefore, equation (1), with n = 1.0, will be used to quantify fluid dynamic behavior occurring at the mouth of the side branch cavity.

It is anticipated that the pressure perturbations existing at the mouth of the side branch cavity will stimulate acoustic resonance propagating along the depth of the cavity. And, since the cavity possesses simple geometry, acoustics mechanics may be applied for modeling the resonance. Resonant frequencies for a pipe with one open end are given by:

$$f_n = \frac{nc}{4W}, \text{ for } n = 1, 3, 5, \ldots \tag{2}$$

where n is the modal number, c is the speed of sound, and W is the pipe depth (Halliday et al., 1993).

The ability for equations (1) and (2) to predict resonant frequencies in systems experiencing flow-acoustic coupling has been demonstrated by Vincent (2000). In this study, a circular pipe and axisymmetric cavity, with length 2.5 in. and depth 0.5 in., was subjected to air flow at U_∞ = 130 fps (Figure 5).

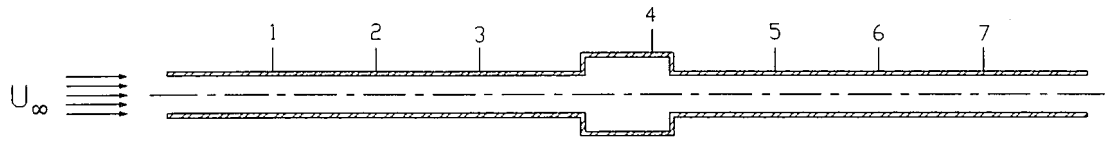

Figure 5 – Sketch of circular pipe and axisymmetric flow system utilized by Vincent (2000). The system was also symmetric about the midpoint of pipe centerline.

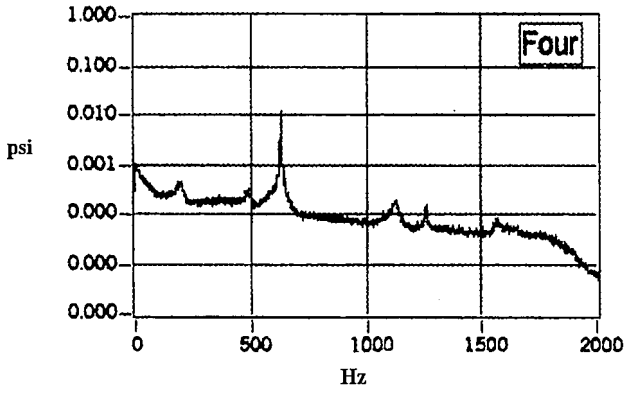

Figure 6 – Pressure spectrum recorded at Station #4 (see Figure 5) illustrates resonant frequency of approximately 625 Hz. The resonance was found to exist with the same magnitude at all stations.

Pressure spectrum data recorded within the cavity revealed a dominant resonant frequency of 625 Hz, which for n = 1.0 resonance, is predicted almost exactly by (1). This resonance was coupled by an acoustical disturbance, which was propagating along the length of each of the adjoining pipes. The resonant frequency, determined by

acoustics analysis, for an analogous pipe with two open ends is given by Halliday et al. (1993):

$$f_n = \frac{nc}{2L}, \text{ for } n = 1, 2, 3, 4, \ldots \tag{3}$$

Given that the total length of pipe, L, was 2 ft and the sound speed was calculated to be 1195 fps (± 5% to account for PIV markers that were entrained in the air flow when the experiment was performed) equation (3) projects mode 2 resonance at 625 Hz with reasonable accuracy. Equations (1) and (2) will be used for anticipating resonant frequencies within the experimental facility.

Similar demonstrations of the validity of equations (1) and (2) to predict acoustic coupling in cavity flows have been performed by Blake (1986), Howe (1997), Rockwell (1983, 1998), and Rockwell & Schachenmann (1982, 1983).

1.4 Existing Quiet Wind Tunnels

Few wind tunnels, which isolate acoustic noise, have been found to exist in published literature. Among these are the subsonic, quiet tunnels at NASA Lewis, Ames, and Langley Research Centers, The CEPRA 19 tunnel in France, The DNW tunnel in The Netherlands (Schmitz et al., 2000, Hall & Woodward, 1996, Schneider & Haven, 1995,

Woodward et al., 1994, and Mosher, 1992), and an experimental facility described by Meyer & Neumann in *Physical and Applied Acoustics* (1972). All of these tunnels, with the exception of that utilized by Meyer & Neumann (1972), employ the same technique of sound attenuation. They employ an anechoic chamber with open jet configuration in the test section. The typical component layout for these tunnels is illustrated by a sketch of the CEPRA 19 tunnel in Figure 7. The tunnel described by Meyer & Neumann (1972) is more like a conventional wind tunnel in the sense that it employs only a porous wall liner in the test section duct to attenuate noise.

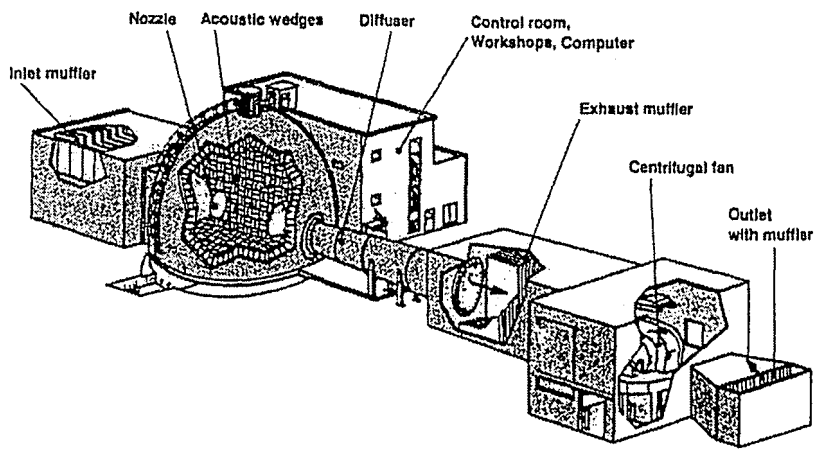

Figure 7 – Schematic of CEPRA 19 quiet wind tunnel, which features an anechoic testing chamber with open jet and collector. (Schmitz et. al., 2000)

As shown in Figure 7, an anechoic chamber is typically a large plenum that is lined with sound absorbing foam wedges. Air flow is brought through the plenum with a nozzle and collector pair that can take extensive research to optimize (Barna, 1995,

1996). The liner used in the Meyer & Neumann (1972) tunnel was described to be a layer of rock wool 75 mm thick that was covered with highly perforated sheet metal on only one wall of a 35 x 100 mm^2 test section. Meyer & Neumann (1972) also describe strategic placement of rock wool at the inlet and outlet of the test section to attenuate incident and suction fan noise respectively. A schematic of the quiet tunnel used by Meyer & Neumann (1972) in their experiments is shown in Figure 8.

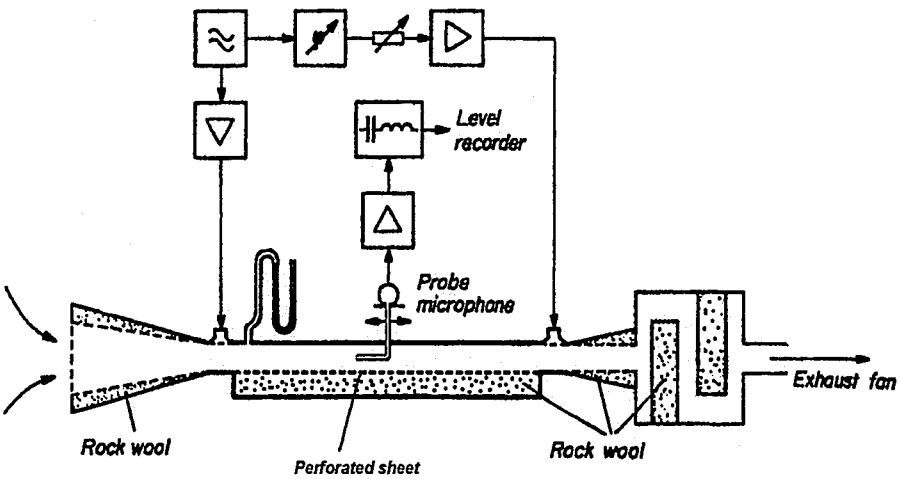

Figure 8 – Schematic of the quiet wind tunnel developed by Meyer & Neumann (1972). It employs highly perforated sheet metal and rock wool insulation on selected inlet, testing, and outlet section walls to attenuate acoustic perturbations.

With consideration of the resources that went into the development of each of these tunnels, it is easy to assume that the anechoic chamber provides a more effective means of isolating acoustic noise. However, the extent to which it is more effective remains questionable. It is also unclear whether the additional attenuation is necessary

for the subject facility and whether including an anechoic chamber in the subject wind tunnel design will be practical with consideration of all facility requirements. A critical evaluation of both quieting methods in parallel with regard to tunnel requirements was performed and is summarized in Section 2.2.

1.5 Quantitative Assessment Techniques

Two measurement techniques are currently being implemented to fully describe fluid flows in experimental research. The first is a method of accurately constructing a two-dimensional instantaneous velocity vector field within any plane of the three-dimensional flow field that is of interest. The instantaneous fields may also be processed to reveal other flow characteristics such as streamlines and vorticity concentration. The second technique involves high speed static pressure sampling and may be utilized simultaneously with the first to reveal instantaneous pressure characteristics corresponding to each of the instantaneous velocity fields.

The first measurement technique is referred to as Particle Imaging Velocimetry (PIV). Its development is attributed to work performed by Adrian, et al. (2000), Adrian (1991), and Adrian, (1986). It involves imaging of a flow field doped with neutrally buoyant markers that are illuminated as they pass through the two-dimensional object plane of a camera. Illumination of the markers is usually performed with high intensity pulsed laser light distributed in a two-dimensional sheet by a cylindrical lens. The

markers used in air flow systems are spherical light-weight oil droplets produced by a machine similar to a carburetor. Their length scale depends on carburetion, but is typically on the order of a micron. Images of the translating markers are taken with digital cameras at framing rates that are presently as high as 30 Hz. Successive image pairs are examined spatially to statistically pair marker images with similar intensity. With the position of the markers relative to the object plane recorded at two successive times, appropriate software constructs a velocity vector field for every pair of images taken during a particular session. A requirement for a PIV installation, besides possession of the necessary hardware, is that the camera object plane be coincident with the sheet illumination provided by the laser. This requires that there be two unobstructed, perpendicular sight lines of the flow field.

The second technique is referred to as static pressure sampling. It involves recording of instantaneous static pressure from high sensitivity transducers that have been fit into an array of wall taps. With hardware that is presently available within the Fluid Mechanics Research Laboratories at Lehigh University, static pressure data may be recorded at the same instant velocity data is taken with PIV. This equipment includes transducers with sensitivity ranging from 1300 to 1600 mV/psi and supporting 30 kHz synchronizer. Together, these instruments permit clear resolution of waveforms with a minimum magnitude of 0.001 psi in the frequency range of 0 to 3 kHz. Sets of instantaneous static pressure are also post-processed with a Fast Fourier Transform, as they have in Figure 6, to reveal resonant frequencies and their magnitudes. An

installation requirement for the static pressure measurement system is that the transducers be seated in taps formed in a rigid wall.

1.6 Facility Specifications

In order to demonstrate that the experimental facility has been adequately designed, it must be capable of exciting the first two resonant modes (n = 1 and 3 in equation (2)) of the flow system as projected by equations (1) and (2). Inherent to meeting this objective is the requirement that all acoustical disturbances besides the resonance propagating along the depth of the side branch cavity be isolated from the vicinity of the cavity mouth. Boundary layers existing on walls adjacent to or opposite the cavity will have to be kept from encroaching on the cavity mouth. And, to accurately characterize the acoustically coupled flow fields, the facility must also support installations of PIV and static pressure measuring instruments.

To measure both free stream and boundary layer velocities at the incipient shear layer (upstream cavity corner), the facility must accommodate a scanning pitot tube equipped with a Linear Displacement Transducer (LVDT) for accurate displacement measurement. Total pressure measurement with the scanning pitot tube should be performed with a calibrated pressure transducer so that velocity measurements can be made without stopping the pitot tube from traversing. It is ideal to also be able to vary the boundary layer thickness at the incipient shear layer.

The cavity length should be of a size adequate to reveal vortex formation and translation within the shear layer using PIV. The cavity depth must be variable in order to determine threshold depths for incipient coupling[1] and to explore excitation at various cavity modes. It is proposed that cavity depth be varied with a suitable plunger arrangement equipped with a micrometer and LVDT for accurate depth and displacement measurements.

The wind tunnel must also fit inside the Air Experiments Laboratory and be driven by an existing 24 inch suction fan that is resident in the laboratory from a former conventional, open-circuit wind tunnel. Detailed performance characteristics of the fan are presented in Section 3.1.

2 PRELIMINARY ASSESSMENT

Satisfaction of all of the facility specifications first requires identification of the parameters that constrain satisfaction of the others. Once identified, a quick assessment of these parameters was made in parallel with facility specifications and tunnel design concepts acquired through literature search. This section serves to present quick

[1] In Section 1.2 it was stated that the determination of threshold *velocities* for incipient coupling was an objective of the present research. However, after combining equations (1) and (2), it can be shown that varying cavity depth produces the same effect on the lock-on condition as varying flow velocity. Varying cavity depth while experimenting is preferred over varying flow velocity because cavity depth can be controlled more precisely.

evaluations of limiting parameters to confirm that adequate resources were provided for meeting facility specifications and to limit the field of possible solutions.

2.1 Adequacy of Existing Suction Fan

Utilization of the existing suction fan imposes a constraint on the range of velocities that will be achievable in the test section of the quiet wind tunnel. The range of velocities that the tunnel must accommodate is mandated by the requirement that the tunnel allows resonance in modes 1 and 3, as projected by equations (1) and (2). Tunnel geometry must be chosen so that the total pressure, or head, that is required for the tunnel does not exceed the head that the suction fan can provide. Some simple calculations were performed at this stage in the design to ensure that the project could continue with the present specifications for the facility. A more thorough assessment of total head (Section 3.1) was performed once the tunnel geometry had become reasonably settled.

The velocities required for excitation of modes 1 and 3 resonance are obtained by the simultaneous solution of equations (1) and (2). Combining these equations yields:

$$\frac{U}{c} = \frac{nL}{4S_n W} \tag{4}$$

By inspection, equation (4) reveals that the upper bound in the required velocity range, U, corresponds to the case where $n = 3$ and $S_n = 1.0$. But, because there was no designation for cavity dimensions with the facility specifications, the cavity depth, W, to length, L, ratio has to be assumed. Figure 9 shows how the required, maximum velocity in the test section varies with cavity geometry.

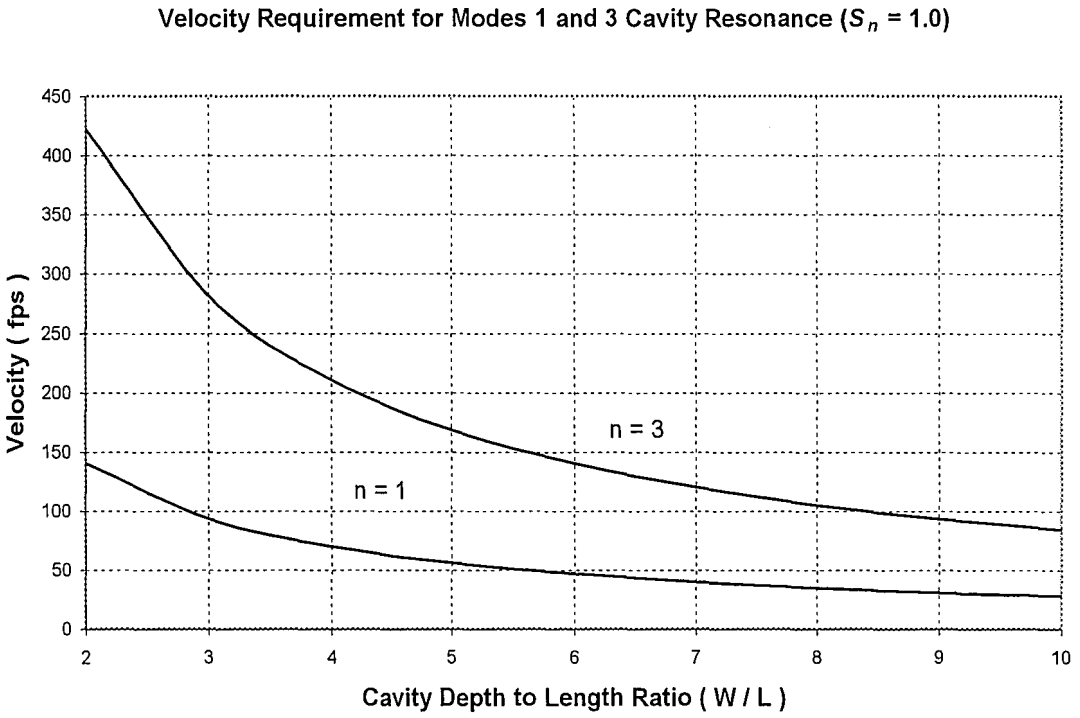

Figure 9 – Variation of required test section velocity for excitation of modes 1 and 3 cavity resonance with cavity geometry.

Familiarity with the PIV systems available within the Fluid Mechanics Research Laboratories suggests that resolution of vortex formation and translation within the shear layer, at the cavity mouth, will be difficult for cavity lengths of less than an inch. This

dimension assumes a camera focal length of 4-5 ft. Increased focal length requires increased cavity length to ensure adequate spatial resolution. With this in mind, a cavity depth to length ratio of 10 was chosen to evaluate whether the suction fan could provide the specified velocity range. A depth to length ratio of 10 was considered to be the limit for incorporating the cavity into the tunnel design without making extraordinary accommodations. It also reduces the maximum required test section velocity, making the existing suction fan more favorable for the application.

With cavity depth to length ratio of 10, the maximum velocity required in the test section, given by equation (4), is 84.5 fps. The suction fan can provide this test section velocity only if the head that it produces at the flow rate corresponding to test section velocity of 84.5 fps is greater than or equal to the total head that is required to achieve that velocity in the test section. Since tunnel geometry has yet to be determined, an assumption of geometry that requires minimum total head will be made for comparison with fan performance.

A wind tunnel duct system that requires the least amount of head is one that has uniform cross-sectional area equal to that of the fan inlet and possesses a preceding gradual inlet contraction. The head required in such a system is that which is necessary to accelerate the flow to the specified velocity plus the head that is dissipated through viscous effects. These quantities are commonly referred to as static load and frictional head loss (or just *head loss*), respectively. Static load and head loss may be approximated by:

$$h_s = \frac{\rho_a}{\rho_w}\frac{V^2}{2}\frac{12}{g} \tag{5}$$

$$h_l = K\frac{\rho_a}{\rho_w}\frac{V^2}{2}\frac{12}{g} \tag{6}$$

where ρ_a and ρ_w are the density of air and water at 68 deg. F respectively, V is the mean velocity, K is a loss coefficient, and g is the gravitation constant. Temperature of 68 deg. F corresponds to the temperature at which fan performance is specified. Both equations (5) and (6) yield customary units 'inches of water' (in. wg.) that may be converted to pressure (in pounds per square foot) according to:

$$P = \rho_w g h_{s,l} \tag{7}$$

The static load necessary to accelerate a flow to 84.5 fps is 1.605 inches of water. To calculate the head loss associated with *dragging* the flow through the gradual inlet contraction and though some length of duct, tables of loss coefficients (presented in Section 3.1.4) were consulted.

Fox & McDonald (1998) give a loss coefficient for the gradual contraction to be 4% of the dynamic pressure, which gives $K = 0.04$. The loss coefficient for a duct with cross-sectional area equal to that of the fan (3.14 ft^2) may be obtained from a Moody

chart (Figure 21). Assuming the duct to have smooth walls and minimum length of 5 diameters (10 ft.), The loss coefficient for this section of the tunnel was determined to be $K = 0.125$. Summing the two loss coefficients and employing equation (6) gives a total head loss of 0.265 in. wg. The total pressure or required head for the simple duct system is therefore 1.870 in. wg., which is substantially less than the 6 in. wg. capacity of the suction fan at the corresponding flow rate of 16,000 cfm (Figure 10). Therefore, it may be concluded that the existing suction fan is capable of supporting the specified velocity range in the quiet wind tunnel.

It is worth noting that, if necessary, fan speed may be reduced so that fan head matches duct head loss. Reducing fan speed is an alternative to venting the tunnel to achieve a target test section velocity. Minimizing fan speed is ideal in the sense that it will minimize noise emanating from the fan and propagating into the tunnel. Fan performance at speeds of less than the manufacturer provided 1398 rpm may be predicted with dimensional analysis (Fox & McDonald, 1998). The relevant scaling equations are:

$$Q' = Q\left(\frac{\omega'}{\omega}\right) \tag{8}$$

$$P' = P\left(\frac{\omega'}{\omega}\right)^2 \tag{9}$$

Where Q, ω, and P denote volume flow rate, fan speed, and suction pressure respectively. The primes denote off-design or scaled quantities. Equations (8) and (9) were employed to map fan performance for several speeds that are less than the design speed of 1398 rpm. The result of which is shown in Figure 11. Confirmation of dynamically safe operation at speeds less than 1398 rpm was made with the fan's manufacturer. Due to fan motor controller limitations, operation of the fan at speeds greater than the design speed is not possible.

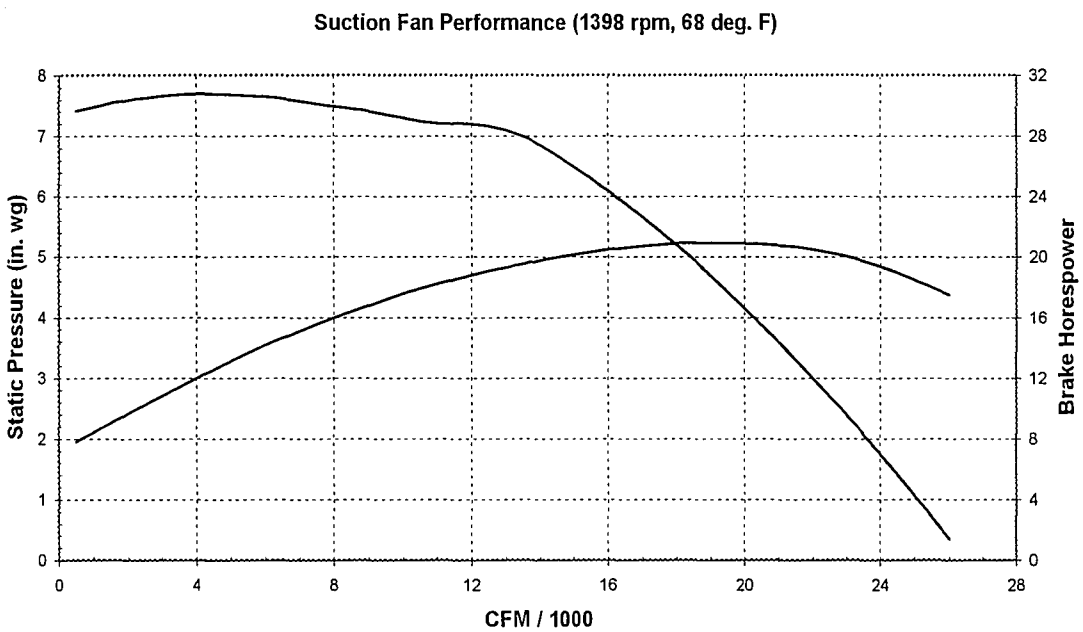

Figure 10 – Performance map for Twin City suction fan model 330 BAF-SW for operation at design conditions. Figure is presented again in Appendix A1. (Twin City Fan and Blower, Minneapolis, Minnesota.)

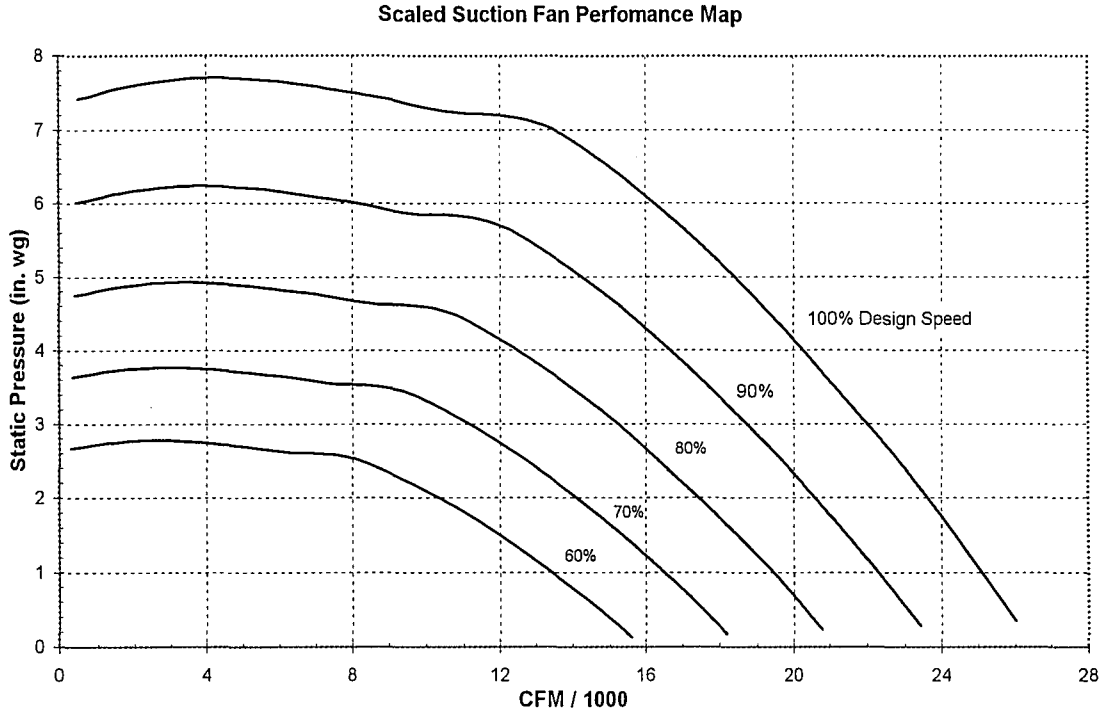

Figure 11 – Suction fan performance at 60, 70, 80, 90, and 100 percent design speed. The scaled performance map is presented again in Appendix A2.

2.2 Discrimination of Potential Solutions

Two different tunnel designs presented in Section 1.3 may be considered viable solutions for the quiet tunnel that is being developed here. The first design has been implemented in facilities that presently exist at major research institutions such as NASA. The design incorporates an open jet and anechoic chamber serving as the testing section of the tunnel. The second design involves the use of porous wall liners to attenuate noise in the test section. This quieting method has been found to exist in only one published

wind tunnel application (Meyer & Neumann, 1972) but, has foundation in noise attenuation techniques that have been used in ducted airflow systems since 1937 (Sivian). At this point in the project, it is necessary to choose which of these designs would be utilized for the subject tunnel.

2.2.1 Discriminating Criteria

The criteria that will be used to evaluate the two tunnel solutions are the facility specifications outlined in Section 1.6. Ideally, the subject tunnel will have high noise attenuation performance, low head requirement (to minimize total energy input to the airflow system), and be able to easily accommodate necessary instrumentation including: a PIV system, pressure transducers, an LVDT for dynamic cavity depth measurement, a traversing pitot tube positioned at the upstream cavity corner for velocity and boundary layer thickness measurement, and a means for varying boundary layer thickness at the cavity mouth.

2.2.2 Attenuation Performance

Meyer & Neumann (1972) determined the noise attenuation performance of their quiet wind tunnel by comparing test section static pressure measurements made both with

and without the acoustically absorbent duct wall liner. The measurements were made while varying tones generated in the test sections with a loudspeaker and while varying air flow velocity and direction. A summary of the measurements is presented in Figures 12 and 13. A similar description of attenuation performance for the quiet tunnels that rely on an anechoic chamber could not be found.

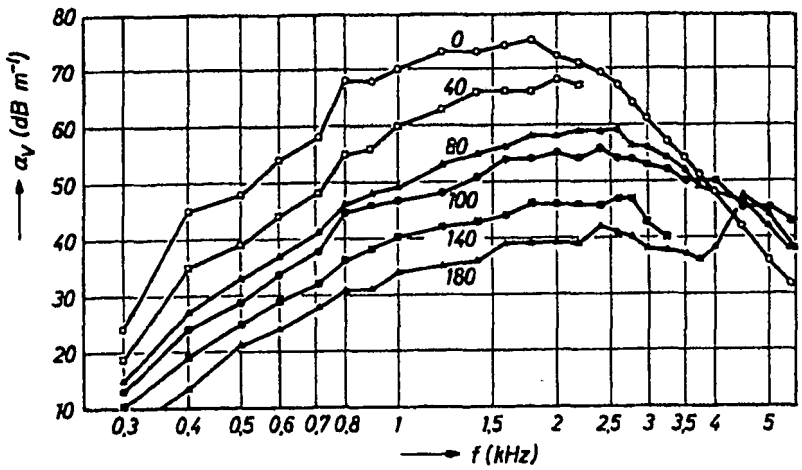

Figure 12 – Attenuation performance of rock wool and perforated sheet liner used on a single wall of the Meyer & Neumann wind tunnel test section with sound propagation in the *same* direction as the air flow. Absorption coefficient is given as a function of frequency and with air flow velocity in meters per second as a parameter. (Meyer & Neumann, 1972)

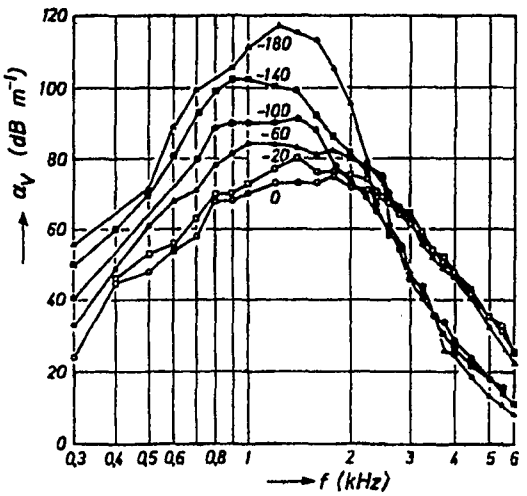

Figure 13 – Attenuation performance of rock wool and perforated sheet liner used on a single wall of the Meyer & Neumann wind tunnel test section with sound propagation in the *opposite* direction of the air flow. Absorption coefficient is given as a function of frequency and with air flow velocity in meters per second as a parameter. (Meyer & Neumann, 1972)

2.2.3 Head Requirement

With regard to head, an anechoic chamber tunnel will require slightly more than the lined wall type tunnel. This realization comes from examination of the plenum-like sections that both tunnels must employ. In order to maintain constant test velocity through the anechoic chamber, continuity requires that the inlet and outlet to the anechoic chamber have the same cross-sectional area. The same restriction is not imposed on the plenum section of the lined wall tunnel however. The outlet area of the plenum section of the lined wall tunnel can be larger than the inlet area of the plenum. Making the outlet

larger than the inlet has a twofold positive effect. It reduces head loss and slows the airflow as it traverses the plenum. Reducing the airflow velocity reduces the kinetic energy of the flow system making perturbations less likely to occur within the plenum.

It is also worth noting that a quiet tunnel possessing an anechoic chamber usually employs three plenum-like sections; one to attenuate inlet noise, one to attenuate test section noise, and one to attenuate suction fan noise (see Figure 7). For the purpose of discriminating between tunnel types with regard to required head, it was assumed that only one plenum-like chamber would be sufficient for attenuating all noise sources. With only one plenum section, the anechoic chamber tunnel possess the same magnitude of head loss as the lined wall tunnel. But with three plenums, the head loss would be substantially greater and would disqualify the anechoic chamber type tunnel from being considered as a potential solution for the subject tunnel. It is questionable, however, whether a single anechoic chamber, with identical inlet and outlet areas, would effectively attenuate fan noise. Greater confidence in tunnel quieting is gained with the use of a plenum section that is dedicated to fan noise attenuation only and is positioned downstream of the testing section because of the difficulty for sound waves to propagate opposite the flow direction (see Figures 12 & 13).

2.2.4 Tailoring the Test Flow

A major discriminating factor between the two tunnel types is their ability to provide and maintain a uniform flow field past the side branch cavity mouth. It is apparent that the flow field in the duct of the lined wall test section and the flow field within the open jet test section of the anechoic chamber will be very different. The most apparent difference between the two flow fields is that of boundary layer thickness. Within the lined wall test section, there will be little growth or thickening of the boundary layer as the flow approaches the cavity because of the favorable pressure gradient within the test section duct. But, because the flow becomes unbounded as it enters the anechoic chamber section, there will exist a zero, or possibly even an adverse, pressure gradient in the open jet flow as it approaches the cavity. This lesser pressure gradient will allow more rapid growth of the boundary layer causing the flow to be less uniform at the cavity mouth.

The possibility of orienting the cavity in the open jet so that neck of the cavity protrudes through the boundary layer and into the uniform region of the flow was dismissed as well, on account of the pressure gradient. It was determined that a zero, and especially an adverse pressure gradient, would permit flow normal to the cavity mouth if a protruding neck was introduced. The only way to reduce the boundary layer thickness in a zero and/or adverse pressure gradient flow, before it reaches the cavity mouth, is with suction provided by an auxiliary flow system. Installing and operating such a system within the anechoic chamber would be difficult.

The open jet will also produce a shear layer between the jet core and the surrounding, recirculating air inside the anechoic chamber. Turbulence occurring in this

shear layer will produce disturbances that will propagate into the jet core unless a suitable nozzle and collector pair are installed at the inlet and outlet of the anechoic chamber (Barna, 1995, 1996). The fact that the quiet tunnel with anechoic chamber solution requires an auxiliary flow system to be installed and operated within the anechoic chamber and development of a nozzle and collector pair makes it less attractive than the lined wall tunnel solution.

2.2.5 Accommodation of Instrumentation

Concerns with PIV system installation are whether both tunnels will able to accommodate two unobstructed, perpendicular sight lines of the flow field for laser projection and digital imaging. Laser projection must occur normal to the cavity mouth so that images may be captured along a side view of the cavity as shown in Figures 1 and 2. Also, of concern is that the distance between the imaging window and the cavity is not so great that image resolution is degraded. This requires that the imaging window be no more than 4 ft. from the cavity mouth for existing cameras to be utilized. This will not be a problem with a lined wall test section, but may be with an anechoic chamber. A quick assessment of required chamber dimensions was performed to make that determination.

The anechoic chamber of Barna (1995, 1996) possessed inlet and outlet area ratios of 7.14. Similar sections of experimental facilities used in the Fluid Mechanics Research Laboratory employ area ratios of 10 or more. Assuming that the tunnel will

operate with the flow rate at which the suction fan produces maximum head (to minimize fan speed), the maximum inlet and outlet areas the anechoic chamber will require can be computed by dividing the volume flow rate of 4000 cfm by 84.5 fps. This yields inlet and outlet areas of 0.789 ft^2. The corresponding anechoic chamber dimensions are obtained by multiplying the inlet and outlet areas by the necessary area ratio. If an area ratio of 10 is assumed (to determine the maximum chamber dimensions), the interior, cross-sectional dimensions of the anechoic chamber will be at most 33.7 inches square. Accounting for acoustically absorbent material that will line the anechoic chamber, the length from the center of the cavity mouth to the outside of the imaging window will be about 20 inches, which is well within the 4 ft. constraint. The pulse-lasers that accompany the imaging systems are so powerful that their projection lengths are not of concern. It was concluded then that installation and operation of a PIV system with an anechoic chamber are easily accommodated.

The same conclusion was not drawn from consideration of the lined wall test section. Windows put through the duct wall linings for laser illumination and imaging are more likely to produce disturbances that will propagate to the vicinity of the cavity mouth because of the larger velocity gradient near the walls and the greater proximity the walls will be to the cavity. The windows will also decrease the available area for wall linings making them less efficient at attenuating disturbances. It was, therefore, concluded that outfitting the lined wall test section with a PIV system poses more of a challenge than does outfitting the anechoic chamber.

The difficulty in installing static pressure wall taps and pressure transducers will be about the same for both tunnel types. These measurement apparatus must be located within a rigid wall of the testing section. For the lined wall section, that wall will be the one in which the cavity resides. The remaining three walls of the test section would possess linings. For the anechoic chamber, the rigid wall, in which the cavity resides, could either be an extension of one of the inlet walls or an island with a sharp leading edge stationed close to the jet centerline. The anechoic chamber will require innovative routing of transducer signal wire, but this is considered to be trivial with respect to the overall installation of pressure measurement equipment.

Equipping the side branch cavity in both tunnel systems with an LVDT to allow dynamic cavity depth measurement does not pose much difficulty either. An LVDT that provides dynamic measurement over the full cavity depth of 10 inches is ideal. This means, however that an additional 10-15 inches of clearance will be necessary at the bottom of the cavity to accommodate translation of the slide portion of the LVDT. The cavity will simply have to branch off of the lined wall test section allowing for unobstructed translation of the cavity floor and will have to be designed to protrude through one of the walls of the anechoic chamber allow for depth variation and accommodation of the LVDT.

Installing and using a pitot tube for total pressure measurement is going to be difficult with both tunnel concepts, but it will be especially difficult with the anechoic chamber. The pitot tube must be able to traverse the flow field at the cavity mouth to reveal boundary layer profiles. Ideally, the pitot tube will be translated from the wall

opposite the cavity and down into the cavity while the tunnel is in operation. What makes installation difficult is that the wall opposite the cavity must have a window to accommodate the laser of a PIV system. Installation and use of the pitot tube is even more difficult with the anechoic chamber because of the 12+ inches that will exist between the cavity and the chamber walls. This distance will inhibit the experimentalist from interacting with the device and its supported hardware directly.

2.2.6 The Choice Concept

After assessing both tunnel concepts with regard to facility specifications, it was determined that: (1) intuitively, the anechoic chamber will better attenuate acoustic noise, but quantitative evidence that demonstrates this could not be found; (2) the effectiveness of a porous wall lined duct has been demonstrated; (3) the lined wall tunnel requires less head than the tunnel that features the anechoic chamber; (4) the lined wall tunnel provides more simplified boundary layer management, and allows for easier accommodation of instrumentation. It was therefore decided that using the lined wall concept for development of the subject tunnel offered greater promise of meeting and/or exceeding facility specifications.

3 DESIGN CONSIDERATIONS AND SOLUTIONS

Having determined which quiet wind tunnel type provides more versatility for meeting project goals, it was then necessary to tailor the winning concept to meet or exceed all facility specifications. This required scrutiny of the lined wall concept with regard to the specifications and the determination of solutions for satisfying or exceeding them. The following passages present this work organized under distinct headings for clarity. The design work itself was performed with simultaneous consideration of all focus areas.

3.1 Fluid Mechanics Considerations

This section presents work that was performed to determine optimal tunnel duct dimensions, how to provide a uniform flow, how to manage boundary layers, and how tunnel performance was modeled. Tunnel layout information is presented first in order to provide a basis for design arguments.

3.1.1 Tunnel Layout

Before additional design work could be addressed, it was first necessary to assign spatial dimensions to tunnel sections. This was an iterative process where dimensions were first assumed then other design considerations evaluated. If, the assumed tunnel

dimensions made satisfaction of facility specifications difficult, the dimensions were reassessed and modified. Major influences on choosing tunnel dimensions were available space and the availability of a pair of surplus inlet contractions.

The room in which the subject tunnel will reside can accommodate a maximum length of 19 ft. for ducted tunnel sections. This figure accounts for a 2 ft. clearance between the tunnel inlet and one of the room walls and for the space that the suction fan already occupies.

Employing the use of surplus inlet contractions is advantageous in development of the subject facility since in-house fabrication of curved contraction walls would be very difficult. The contractions are composite fiber and resin material formed from a template or mold containing the specified curvature. Additional incentive for using the surplus contractions was gained after receiving cost quotations in the amount of $1500 each for the purchase of two new ones. A layout of the interior wall lines of the proposed tunnel is shown in Figure 14.

Section A of Figure 14 is contraction 1 of the surplus pair and has interior cross section that converges from infinite area to 30 inches square. Section B is a flow straightener (described further in section 3.1.2). Section C is contraction 2 of the surplus pair and has cross section that converges from 30 inches square to 8 inches square. Section D is the test section and possesses interior cross section of 8 inches square. Section E is a diffuser with two dimensional divergence from 8 inches square to 15 inches square. Section F is a plenum containing acoustic baffles, G, that attenuate the

upstream propagation of fan noise. Section F has interior cross section of 44 inches square. Section H is an additional flow straightener (addressed in section 3.1.2).

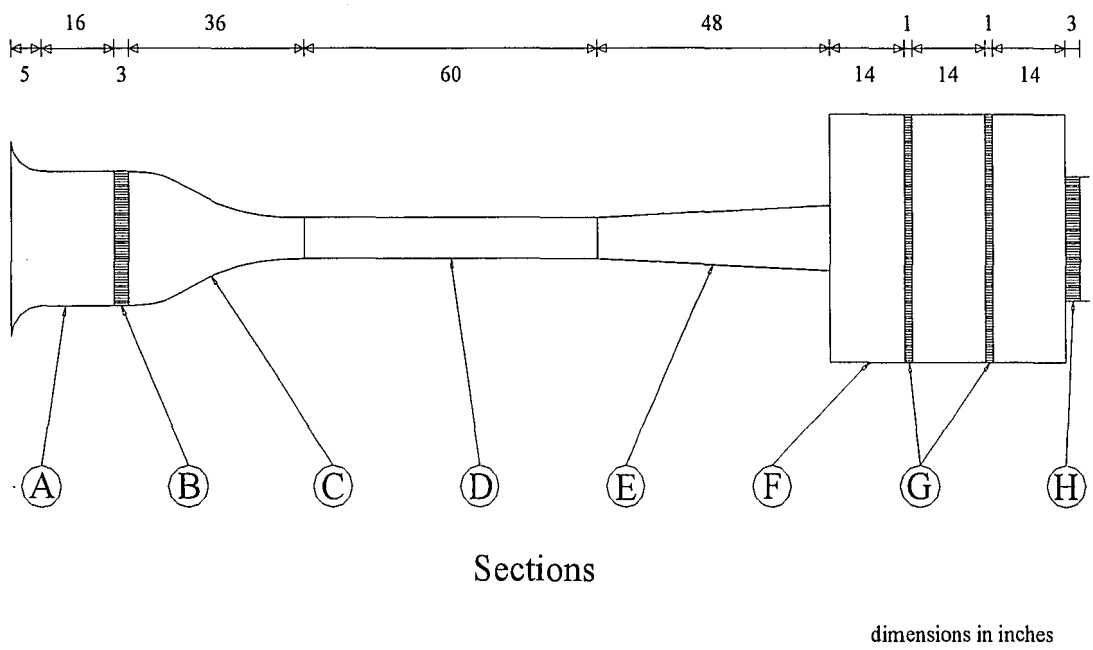

Figure 14 – Sketch of tunnel interior geometry shown with sections drawn to scale. Figure is presented again in Appendix A3.

The diffuser was included in the tunnel layout since there was available space for it and because it reduced tunnel head loss sustained at the plenum inlet. The diffuser possesses two-dimensional divergence and an area ratio of 3.5. Its dimensions were selected based on empirical diffuser performance data collected by Runstadler, et al. (1975) and iterative calculation of head loss.

Plenum cross-sectional dimensions were chosen under the size constraint of Section G so that the area ratio between Sections E and F was equal to 8.6. Plenum

length was chosen cooperatively with test section and diffuser lengths so that all of the tunnel sections would fit inside of the maximum 19 ft. available space.

3.1.2 Flow Uniformity

A uniform flow field will be maintained outside of the boundary layers in the test section by employing a flow straightener between the two stages of inlet contractions. A flow straightener acts to break-up any turbulence or rotational flow induced by the first contraction at the tunnel inlet. Honeycomb core is routinely used for flow straighteners in wind tunnel and water channel applications. It will serve as a flow straightener in the subject application as well. In order to determine the size and type of core to be used, attention was given to the core that was used as a flow straightener in the existing conventional wind tunnel.

Contraction 1 of the larger, conventional wind tunnel the subject facility will be replacing possessed cross section that converged from infinity to 45 inches square. Contraction 2 reduced flow area from this dimension to 18 inches square. An aluminum core that possessed cell size of 3/8 inches and depth of 3 inches was used between the two contractions as the flow straightener. The ribbon thickness of the core was 0.004 inches.

The area ratio between the outlet of contraction 1 and a single core cell was used to determine the appropriate cell size for the smaller, quiet wind tunnel contractions.

Assuming the hexagonal cells of the conventional wind tunnel honeycomb core to be circular with diameter equal to the cell size gives an area ratio of 4584. A cell size of 1/4 inches would therefore be necessary to achieve this ratio with inlet contraction 1 of the quiet tunnel.

Core cell areas were also compared with contraction 2 outlet areas. Contraction 2 of the larger tunnel possessed an area ratio of 733 while contraction 2 of the quiet tunnel possessed an area ratio of 326. The lower area ratio is desirable since it implies that the flow will be contracted further than it was through the conventional wind tunnel inlet sections. The additional contraction will make the flow more uniform and less likely to become rotational.

To determine the appropriate thickness for the new core, the length ratio of core thickness to cell size for the core that was used as a flow straightener between the contractions in the larger, conventional tunnel was considered first. The 3/8 inch cell core possessed 3 inch thickness, which gives an *L/D* ratio of 8. This is shy of the standard ratio of 10 that is used to characterize fully developed internal flows. It is assumed that the ratio of 8 was employed rather than 10 to reduce velocity variations at the trailing edge of the individual core cells. It is further assumed that any disturbances formed as a result of velocity variation at the trailing edge were dissipated while passing through contraction 2. These assumptions coupled with the fact that the quiet tunnel will possess a contraction 2 outlet area to core cell area ratio that is less than half of what was employed for the conventional tunnel provided encouragement for specifying a core

thickness that produced an *L/D* ratio greater than 8. This was an important revelation considering that an *L/D* ratio of 8, with 1/4 inch core, requires thickness of 2 inches.

Reluctance was expressed for specifying a 2 inch core thickness because it was anticipated that a 1/4 by 2 inch core would deflect and/or vibrate under drag loading imposed by the maximum flow rate the fan could sustain through the tunnel. The drag loading could be estimated by calculating the head loss through the core at the maximum flow rate. The load, which was determined to correspond to the tunnel flow rate of 6500 cfm, was calculated from empirical data provided by the core vender to be 0.003 psi. Calculation of the deflection the core would sustain as a result of the drag load was considered at this point, but parameters required for the calculation (elastic modulus and bending moment of inertia for unstabilized 1/4 inch core) were not provided by the vendor. Therefore, deflection of the core as it is subjected to the maximum tunnel flow rate could not be determined analytically.

To compensate, core thickness of 3 inches was specified for the 1/4 inch honeycomb core. It was determined that the extra rigidity the added inch provides is worth the additional head loss for prevention of core vibration under the maximum flow condition. Additional vibration countermeasures include pressing (over expanding) the core to fill its supporting frame and positioning of compliant wall lining foam so that it lies adjacent to the core.

It was, at last, necessary to specify the alloy type and foil thickness of the core. Ideally, the foil would be as thin and as strong as possible in order to minimize trailing edge disturbances and pressure drag. However, thin foil makes the core both difficult to

handle and less rigid. Cores made from the stronger alloys were also more expensive than the those made from the standard aluminum alloys mainly because of the quantities in which they were produced not performance under loading. Negotiating these concerns with the vendor, 5052 aluminum foil was chosen with thickness of 0.0015 inches. The core also received an inexpensive anodyne treatment for corrosion resistance. Mechanical properties of Hexcel 5052 aluminum honeycomb cores are presented in Appendix A4.

3.1.3 Boundary Layer Management

The objective in boundary layer management is to tailor the flow in the test section so that characteristic boundary layer thicknesses at the upstream edge of the cavity mouth are as thin as possible. These characteristics include the boundary layer thickness, δ, displacement thickness, δ^*, and momentum thickness, θ. Before the boundary layer attached to the wall possessing the cavity could be manipulated however, it was first necessary to determine its characteristic lengths.

Boundary layer characteristics for the turbulent internal flow that will occur within the test section can not be determined analytically. Therefore, it would be necessary to research published experimental data for internal flows with the same Reynolds number to accurately specify boundary layer characteristics in the test section. Instead of engaging in this laborious and tedious task, it was determined that managing

the boundary layer could be performed more practically if maximum thicknesses were identified.

A turbulent boundary layer has characteristic thicknesses that are less than those for a laminar boundary layer. And, a boundary layer existing in a flow with a favorable pressure gradient has characteristic thicknesses that are less than those for a boundary layer existing in a flow with a zero pressure gradients. With these facts in mind, it was determined that boundary layer thickness characteristics for flat plate flow with zero pressure gradient (Blasius flow) provide an upper bound for the test section boundary layer characteristics. And, designing under the assumption of maximum characteristic thickness would ensure that the actual, test section boundary layer characteristic thicknesses are much less if not null.

Boundary layer characteristics for Blasius flow are given by the following:

$$\delta = \frac{5x}{\sqrt{\mathrm{Re}_x}} \tag{10}$$

$$\delta^* = \frac{1.72x}{\sqrt{\mathrm{Re}_x}} \tag{11}$$

$$\theta = \frac{0.664x}{\sqrt{\mathrm{Re}_x}} \tag{12}$$

Equations (10) through (12) all assume the edge of the boundary layer to be where u/U_∞ = 0.992. Using equations (10) through (12), maximum boundary layer thickness, displacement thickness, and momentum thickness occurring in the test section were determined as a function of test section velocity. A plot of the three functions is shown in Figure 15.

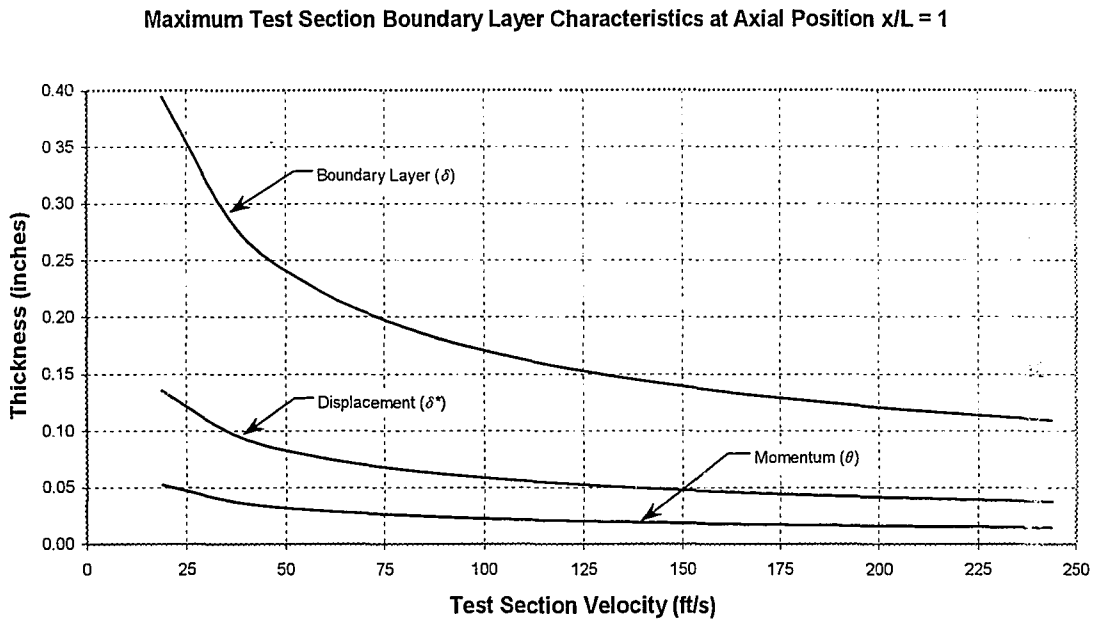

Figure 15 – Illustration of boundary layer characteristic thickness for flat plate flow with zero pressure gradient. Reynolds number based on the entire test section length of 5 ft. was used. Figure is presented again in Appendix A5.

Upon inspection of Figure 15, it should be noted that boundary layer characteristic lengths decrease with increasing test section velocity. And, from Figure 9, cavity depth necessary to achieve resonant frequencies also decreases. Rates of change

between the two are insignificant since Figure 15 provides only an upper bound for boundary layer characteristic lengths. It should also be noted that while boundary layer characteristic lengths and required cavity depth decrease with increasing test section velocity, fan noise and the likelihood that the noise will propagate into the test section *increases* with test section velocity. Therefore, it is not possible to specify an optimal test section velocity based on the Figures 9 and 15.

Based on Figure 15 it may be possible, however, to specify a protrusion height for the neck of the cavity as a function of velocity so that boundary layer characteristic lengths are all zero. The favorable pressure gradient within the test section may prevent flow normal to the cavity mouth that would otherwise exist in its absence. A compression wedge prior to the cavity neck may also be of use in minimizing boundary layer characteristic lengths and/or preventing flow normal to the cavity mouth. Experimental measurement of the boundary layer at the cavity mouth will have to be performed to know for sure.

3.1.4 Tunnel Head Requirement

The most significant influence on tunnel duct layout and dimensions was velocity and head calculation. The objective here was to use available correlations and head loss data to compute tunnel head requirement as a function of test section velocity and to ensure the existing suction fan could still drive it. To accomplish this objective, the tunnel duct system was assigned eight stations at which static load and head loss were to

be calculated with use of equations (5) and (6) based on the mean velocity at each of the stations (Figure 16). Tunnel flow rates were first assumed then mean velocities were calculated with continuity. All tunnel head calculations were performed using air properties at the same temperature for which fan performance was provided; 68 deg. F. Loss coefficients were determined based on charts provided by Fox & McDonald (1998), which are shown in Figures 17, 20, 21, 22 and 23.

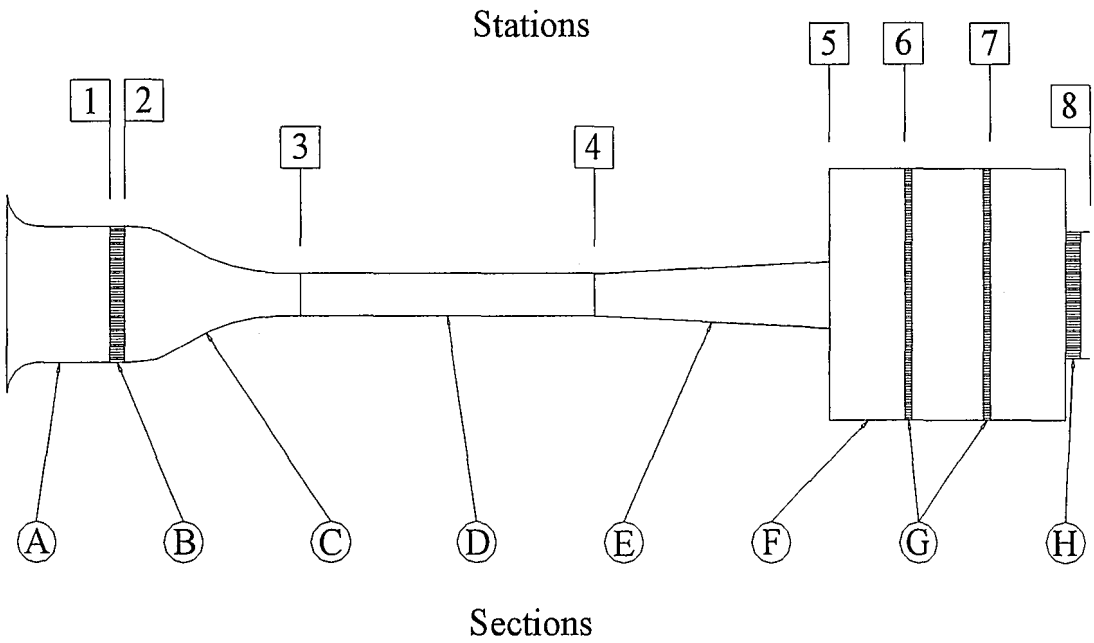

Figure 16 – Illustration of station assignment for calculation of total head. Figure is presented again in Appendix A6.

The static load at Station 1 was computed with equation (5) based on velocity obtained with continuity. Air velocity outside of contraction 1 was assumed to be zero.

The loss coefficient for Section A was estimated to be $K = 0.04$ with the use of Figure 17. There is no change in static load from Station 1 to Station 2 since the cross-sectional area of the duct does not change. The head loss that occurs from Station 1 to Station 2, as a function of velocity, had to be interpolated from experimental data provided by the honeycomb core manufacturer (Hexcel). The data is shown in Figure 18. Interpolated data points were taken from Figure 18 and used in a regression routine to obtain head loss as a function of velocity. The results of the correlation are shown in Figure 19.

Entrance Type		Minor Loss Coefficient, K^a
Reentrant	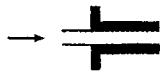	0.78
Square-edged		0.5
Rounded		r/D | 0.02 | 0.06 | ≥ 0.15 K | 0.28 | 0.15 | 0.04

[a] Based on $h_{L_m} = K(\bar{V}^2/2)$, where $\bar{V}$ is the mean velocity in the pipe.

Figure 17 – Loss coefficients for inlets with various geometry. (Fox & McDonald, 1998)

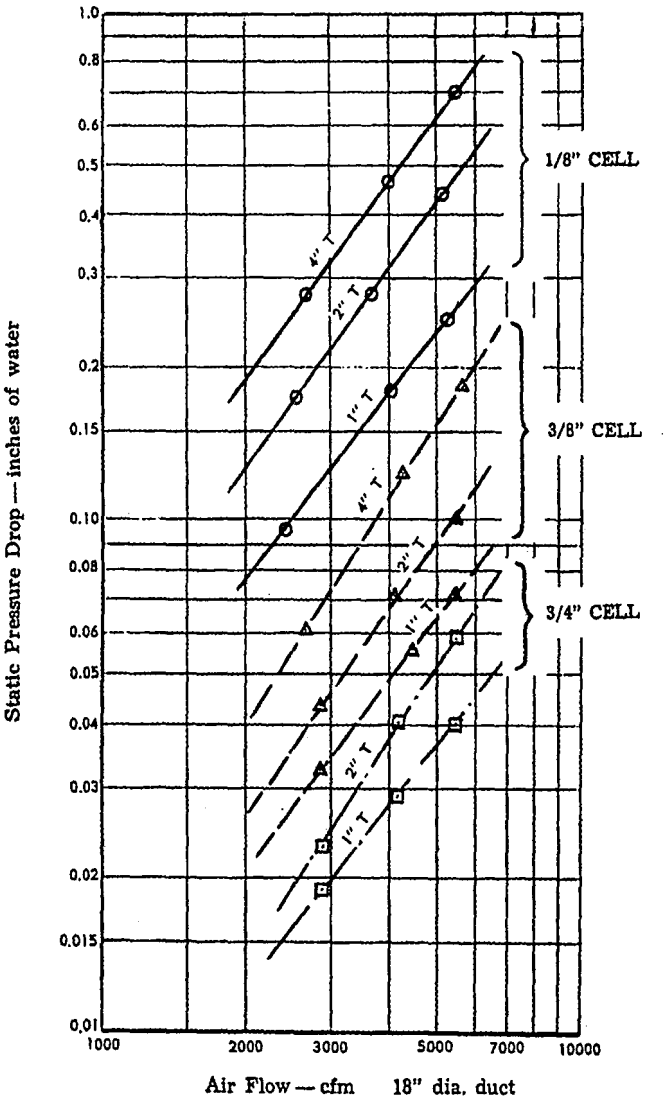

Figure 18 – Head loss data for aluminum honeycomb core of various cell sizes and thicknesses as a function of velocity (Hexcel). Figure is presented again in Appendix A7.

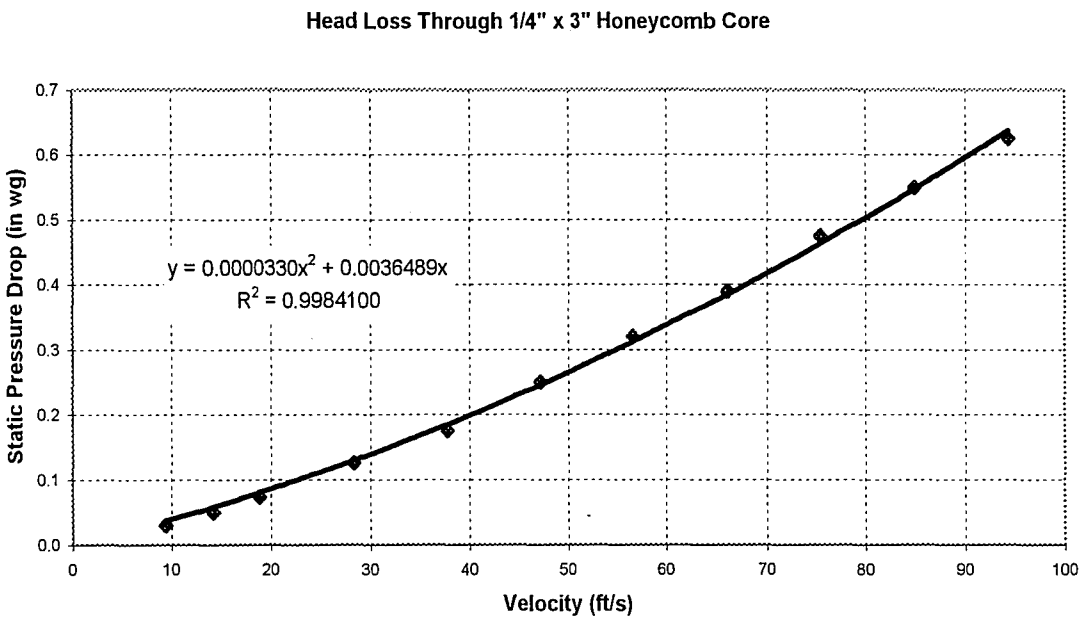

Figure 19 - Functional relationship between static head loss and inlet velocity for flow straightener. Function was obtained with regression of manufacturer supplied data. Figure is presented again in Appendix A8.

The static load required to accelerate the flow from Station 2 to Station 3 was calculated again with equation (5) and the equation of continuity. The loss coefficient was estimated to be $K = 0.05$ from Figure 20. There is no change in static load from Station 3 to 4. Loss coefficient for Section D was determined from:

$$K = f\frac{L}{D} \tag{13}$$

where f is obtained from the Moody chart (Figure 21) for smooth pipes, L and D are the length and diameter of Section D, respectively.

	Included Angle, θ, Degrees							
	A_2/A_1	10	15–40	50–60	90	120	150	180
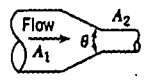	0.50	0.05	0.05	0.06	0.12	0.18	0.24	0.26
	0.25	0.05	0.04	0.07	0.17	0.27	0.35	0.41
	0.10	0.05	0.05	0.08	0.19	0.29	0.37	0.43

Note: Coefficients are based on $h_{L_m} = K(\bar{V}_2^2/2)$.

Figure 20 – Loss Coefficients for gradual contractions. (Fox & McDonald, 1998)

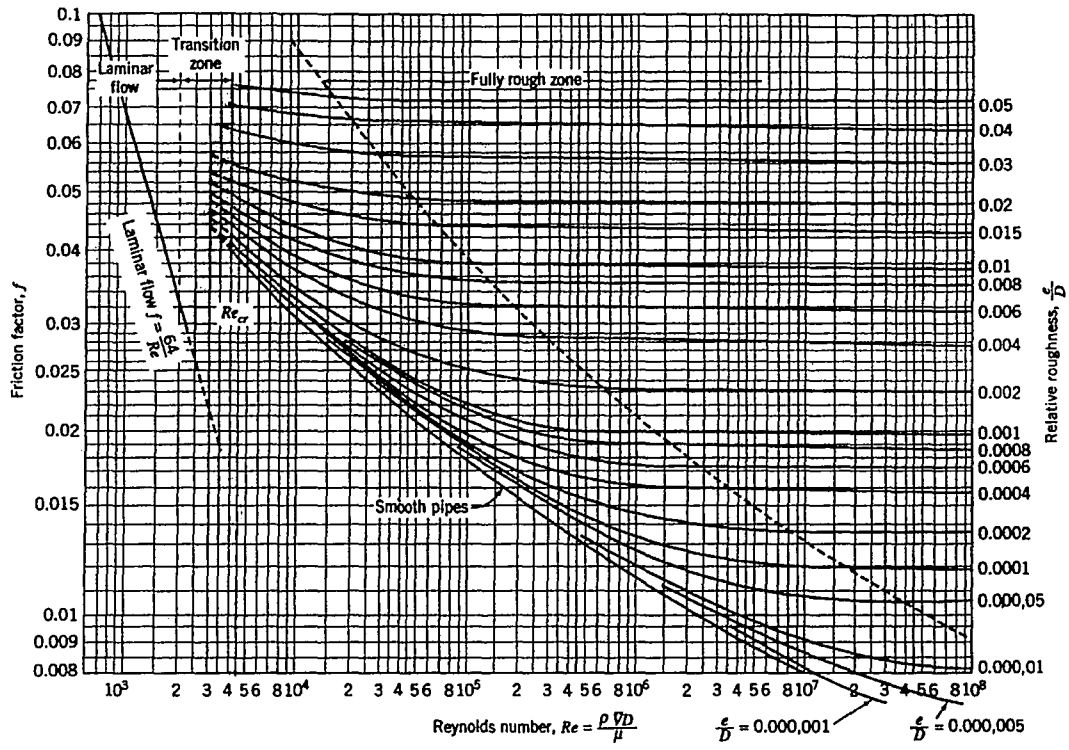

Figure 21 – Moody chart for evaluation of duct friction losses as a function of Reynolds number (Fox & McDonald, 1998). Figure is presented again in Appendix A9.

The diffuser, Section E, was added to the tunnel layout because of the significant reduction in head loss that it offered and the availability of space to accommodate it. The diffuser was designed with two-dimensional divergence based on empirical data collected by Runstadler, et al. (1975) for conical diffusers (Figure 22) and the hydraulic diameter analogy. Given that there was 50 inches of available, axial length for the diffuser and that the outlet of the test section was to be 8 inches square, various area ratios were investigated for minimum head loss before the final selection of 3.5 was made. The pressure recovery coefficient, C_p, for $N/R_1 = 6.25$ and $AR = 3.5$ was estimated to be 0.57.

The static pressure gained through the diffuser was calculated with the continuity equation. Head loss through the diffuser section was calculated according to:

$$h_l = (C_{p,i} - C_p)\frac{\rho_a}{\rho_w}\frac{V^2}{2}\frac{12}{g} \tag{14}$$

where V is the mean velocity at the inlet of the diffuser and $C_{p,i}$ is the ideal pressure recovery coefficient determined by:

$$C_{p,i} = 1 - \frac{1}{(AR)^2} \tag{15}$$

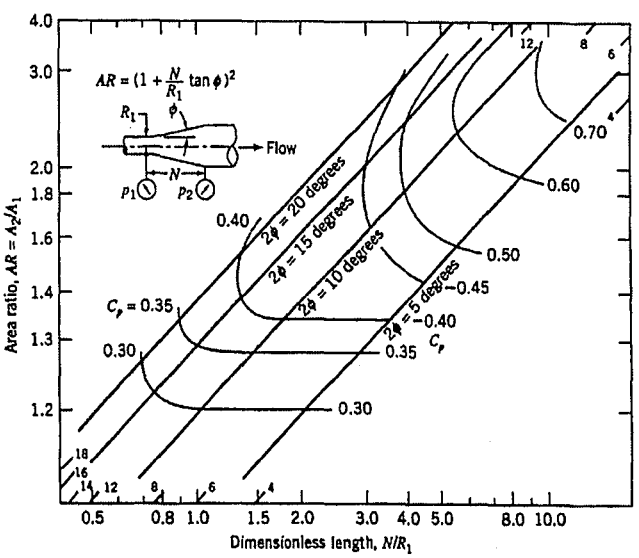

Figure 22 – Pressure recovery for conical diffuses with fully developed turbulent inlet flow (Runstadler et al., 1975 reprinted by Fox & McDonald, 1998). Figure is presented again in Appendix A10.

Static head gained from Station 5 to Station 6 was calculated using equation (5) and continuity. Head loss occurring between Station 5 and Station 6 was calculated using equation (6) and Figure 23. For an area ratio of 8.6, the loss coefficient for flow between Stations 5 and 6 was estimated to be $K = 0.8$.

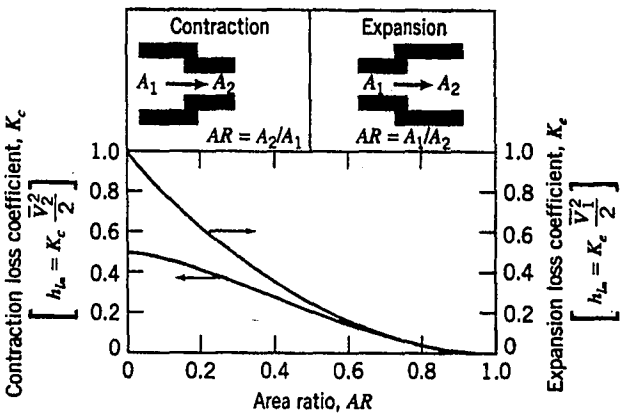

Figure 23 – Loss coefficients for abrupt contractions and expansions. (Fox & McDonald, 1998)

The head loss across the 2 filter-style baffles at Stations 6 and 7 was determined as a function of inlet velocity as it was for the flow straightener (Section G). However, the supplier of the baffles was unable to provide test data for head loss. The supplier was able to confirm only one data point for head loss across the baffles. Air filters Inc. (Texas) quoted that the head loss across the baffles would be 0.2 in. wg. for new filters experiencing flow velocity of 5 fps. These values were substituted into equation (6) in order to determine the loss coefficient K so that a functional relationship for head loss

and flow velocity could be obtained for the baffles. The value of K, in equation (6), which yields head loss of 0.2 in. wg. per baffle with 5 fps incident velocity is 36.19. There is no change in static load across Stations 6 and 7 since there is no change in cross-sectional area.

Head loss that occurs from Station 7 to Station 8 due to the sudden contraction was estimated with the use of equation (6) and Figure 23. With area ratio of 0.23 between Sections H and G, Figure 23 shows K to be approximately equal to 0.4. Head loss that occurs from the flow straightener was estimated with the function obtained from correlation of experimental data, which is shown in Figure 19. The static load required to traverse Station 8 was computed with equation (5) and continuity.

Tabulated numerical head loss and static load data is presented in Appendix A11. The table contains performance data for the tunnel duct system with and without the diffuser. The same data is presented in graphical form in Figure 24. The official tunnel performance map which gives fan head and tunnel head requirement as a function of test section velocity is presented in Figure 25.

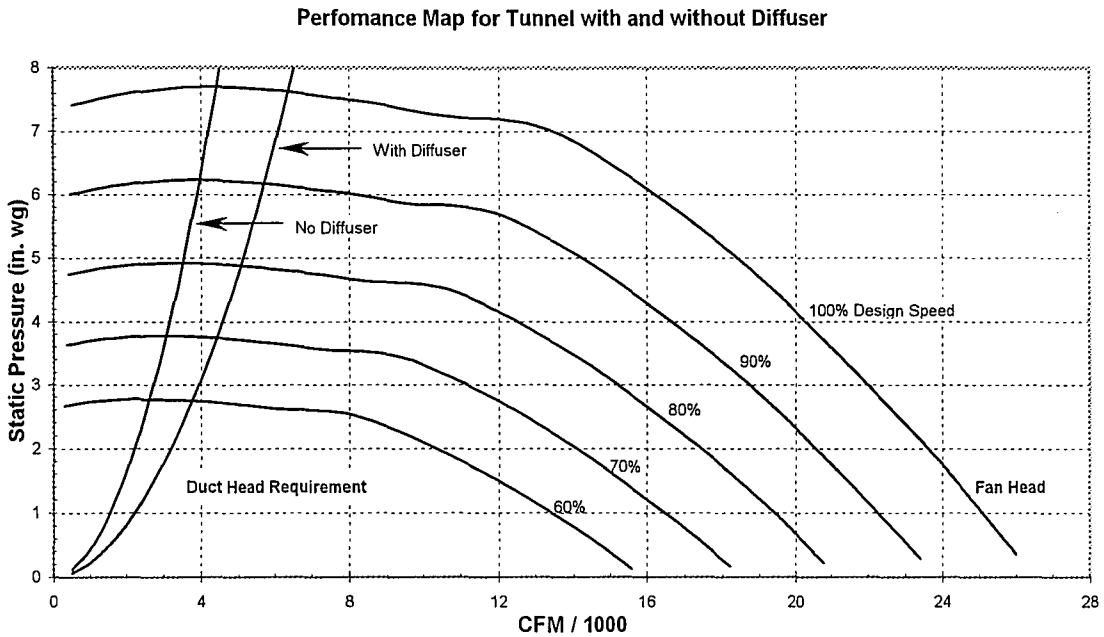

Figure 24 – Illustration of scaled fan performance with corresponding head requirement for tunnel duct system possessing diffuser and tunnel duct system without diffuser. Required head curve on right corresponded to tunnel system with diffuser (final design). Figure is presented again in Appendix A12.

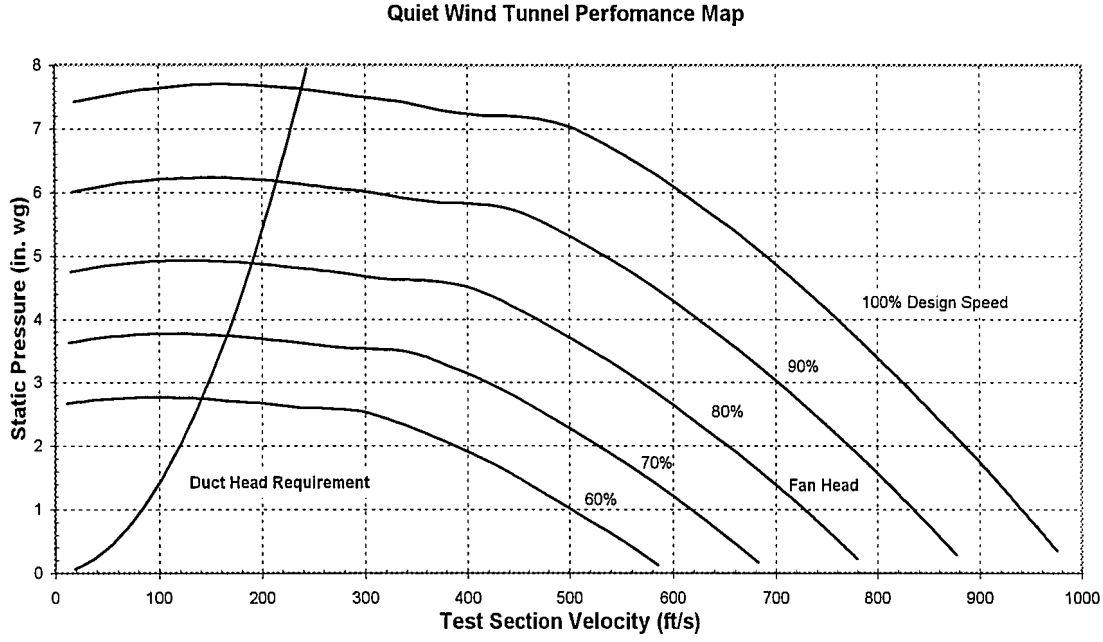

Figure 25 – Quiet wind tunnel head characteristics as a function of test section velocity. Figure is presented again in Appendix A13.

3.2 Acoustics Considerations

This section presents work related to the selection of the wall lining to be used in the quiet tunnel and the method by which fan noise is to be controlled. The work is organized into discussions specific to acoustic absorber characteristics, tunnel acoustic requirements, absorber candidates, and the tunnel acoustic solution. The discussion on general characteristics of acoustic absorbers is presented first.

3.2.1 Acoustic Absorber Characteristics

Acoustic absorbers are low density materials that dissipate periodic pressure perturbations that are inherent to sound waves. Absorbers that are both pervious and impervious to air flow were explored for use in the quiet tunnel. Pervious absorbers, or the filter-type baffles mentioned in Section 3.1 were explored for use in the plenum section to attenuate fan noise. Impervious absorbers were explored for use as linings on all of the interior walls of the tunnel to attenuate flow induced noise.

While searching for performance characteristics of acoustic absorbers, it was discovered that both types of absorbers are commercially available but, neither type has been developed for wind tunnel applications. That is to say, impervious absorbers developed as wall linings have not been designed for or tested in applications where they are subject to high speed tangential flow. They have been designed for and tested in applications possessing static air instead. And, pervious absorbers have not been designed for attenuating sound propagation in the direction of air flow, but rather for the filtration of particulates. It was, therefore, necessary to study derivatives of each absorber type and to use ingenuity in making available absorbers effective in the present application.

An alternative to implementing a commercially available acoustic absorber as a wall lining in the quiet tunnel, was the development of a lining similar to the one used in the tunnel described by Meyer & Neumann (1972). Their tunnel employed highly perforated steel sheet covering rock wool insulation as a wall lining. This technique is

routinely used to attenuate sound in high speed, high temperature flow systems such as internal combustion engine exhaust systems.

Most of the commercially available acoustic absorbers discovered were porous polymer foams. The foams possessed a variety of surface geometries, densities, and thicknesses. The characteristic that was common to all foams found was the Random Incidence Acoustical Absorption Coefficient (RIAAC), which is a measure of absorbed sound energy divided by incident sound energy at 125, 250, 500, 1000, 2000, and 4000 Hz, in accordance with ASTM C423-84 and E795-83.

The commercially available acoustic foams possessed explicit RIAAC designations. This allowed for quick evaluation of the variety of available acoustic foams to distinguish candidates for the tunnel application. The same performance characteristic was not as easily accessible for rock wool type liners. Because rock wool liners are designed specifically for their particular applications, attenuation performance standards such as ASTM RIAAC have yet to be established for these liner types. While attenuation performance is available for the rock wool liner used by Meyer & Neumann in Figures 12 and 13, the performance is limited to a tunnel system with the same acoustic properties (duct resonant frequencies). On the other hand, this performance includes air flow effects. The RIAAC for commercial acoustic foams is valid only for static air.

It was necessary to evaluate both of these impervious absorber types, as well as various pervious absorbers, for the quiet tunnel application but, specific tunnel requirements had to be identified first.

3.2.2 Tunnel Acoustic Requirements

The objective of the acoustic absorbers is to attenuate noise within the wind tunnel duct system. Noise sources which are anticipated to exist within the tunnel include: the suction fan, axial acoustic mode of the test section, transverse acoustic mode of the test section, and acoustic mode of the side branch cavity. In order to identify acoustic absorbers that will effectively attenuate noise emanating from all of these sources, it was first necessary to project source frequencies since absorber attenuation performance is frequency dependent.

The suction fan will be a significant source of noise in the tunnel, especially at the upper end of its range of capable speeds. It is difficult to isolate a particular frequency for which fan noise will be dominant since there is no baseline static pressure spectrum available for the previous, rigid walled tunnel that the fan was a part of. Therefore, it was assumed that fan noise would have uniform intensity over the 100 to 4000 Hz range and that an absorber with good attenuation properties over the entire range of these frequencies would be necessary.

Projection of sound frequencies that will be generated from air flow past the cavity may be performed with equations (1), (2), and (3). Periodic vortex formation and impingement at the side branch cavity mouth can couple with one of the acoustic modes of the side branch cavity, an axial mode of the test section duct, and/or a transverse mode

of the test section duct. Depending on the test section velocity, dynamic fluid behavior at the cavity mouth may couple with all three acoustic modes.

The range of tones that will be generated by the side branch resonator was limited by first identifying both axial and transverse modes of the test section. Axial modes were determined to occur every 112.6 Hz using equation (3) and test section length of 5 ft. Transverse modes were determined to occur every 845.5 Hz using equation (3) and test section width of 8/12 ft. The harmonics for a closed-closed resonator are the same as those for a open-open resonator (Halliday et al., 1993).

Cavity modes were then tabulated for $n = 1$ and $n = 3$ resonance, as a function of cavity depth to length ratio W/L, with the use of equation (2). The ratio, W/L, was assumed to range from 2 to 10 and cavity length was assumed to be 1 inch for brevity. Cavity resonance at integer values of W/L were then substituted into equation (1), with $S_n = 1.0$, to determine the velocity required for flow coupling to occur with the cavity modes. The upper bound on the frequency of noise generated in the test section was then determined by the maximum achievable velocity in the test section. Figure 25 shows that the duct head requirement curve intersects the fan head curve for 100% design speed at nearly 250 fps test section velocity. The range of frequencies needing to be attenuated in the test section, therefore, correspond to 0-250 fps. From Figure 26 this range was identified to be 112.6 to 2533.5 Hz.

	Cavity Modes				Lock-on Velocity	
W/L	(n = 1) (Hz)		(n = 3) (Hz)		(n = 1) (fps)	(n = 3) (fps)
2	1689.0	(A)			141	
3	1126.0	(A)			94	
4	844.5	(T)	2533.5	(T)	70	211
5	675.6	(A)	2026.8	(A)	56	169
6	563.0	(A)	1689.0	(T)	47	141
7	482.6		1447.7		40	121
8	422.3		1266.8		35	106
9	375.3		1126.0	(A)	31	94
10	337.8	(A)	1013.4	(A)	28	84

Figure 26 – Tabulation of resonant cavity frequencies and corresponding lock-on test section velocities at integer values of *W/L*. Frequencies shown with an (A) are also axial modes of the test section duct. Frequencies shown with a (T) are also transverse modes of the test section duct.

It is difficult to project the magnitude of resonance that will occur in the test section analytically. Experiments performed by Vincent (2000) showed that the amplitude of cavity resonance coupled with axial resonance of the supporting duct was a factor of 10 psi greater than the pressure spectrum for uncoupled behavior. It is assumed that a similar condition will exist when cavity modes are coincident with axial test section modes. It is unclear whether resonance amplitude will increase again at 1689 Hz, where the cavity mode and axial test section mode are coincident with the transverse test section mode. It is safe to say however, that test section resonance at 1689 Hz will be more easily excited than other cavity frequencies.

In addition to identifying frequency requirements for potential absorbers, mechanical properties needed to also be identified. Acoustic absorbers lining the interior walls of the wind tunnel walls must not deflect or ripple when exposed to tangential flow

with speeds of up to 250 fps. Deflection of the absorber surface resulting from flow induced tangential shear may cause unsteady pressure fluctuations with amplitude that is greater than flow-acoustic locked modes.

3.2.3 Absorber Candidates

There are two acoustical absorber types that were considered for use as a linings on the tunnel walls. They include the rock wool and perforated sheet covering similar to the one that was implemented by Meyer & Neumann (1972), and a commercially available acoustic foam. Influencing the usage of the rock wool and perforated sheet covering is the fact that it is a proven effective noise attenuation technique used in the Meyer & Neumann (1972) tunnel, as well as, other flow systems – most of which are high temperature applications. Drawbacks to its usage are that it would be more expensive and more difficult to implement than an acoustic foam and that there is a possibility particles of the insulating material could be entrained in the airflow and exhausted into the laboratory.

Influencing the usage of an acoustic foam is that the foam can be quickly and easily cut to size from sheet stock and applied to tunnel walls with available pressure sensitive adhesive backing. Another advantage of an acoustic foam is that some foams are available with laminated 1 mil polyester facings, which will prevent the foam from absorbing oil particles used for PIV. The attenuation performance of both the rock wool

and acoustic foam absorbers would be detrimentally affected should the absorbers contract oil. Samples of acoustic foam candidates were obtained to certify that the acoustic foam would not deflect or ripple when exposed to tangential flow with speeds that will exist in the test section.

There was a limited selection available for pervious absorbers that could be used to attenuate fan noise. The only class of pervious absorber found were foam filter elements used in HVAC applications. And, while no sound attenuation characteristics were solicited with these types of absorbers, it is anticipated that a filter possessing a thick section of firm foam will perform well inside of the plenum section.

3.2.4 Tunnel Acoustics Solution

A polyether urethane acoustic foam with 2 inch thickness and manufactured by EAR Specialty Composites (Newark, DE) was chosen for use a wall liner in the quiet tunnel. Its physical properties and acoustic attenuation performance are shown in Figure 27. The baffles chosen for use at Stations 6 and 7 are 3 ply foam filter elements with overall thickness of 1 inch. The plies have graduated density and porosity with the upstream ply being the most porous and least dense. The filters were provided by Airfilters Inc. (Houston, TX).

Tufcote Polyether Urethane Foam Typical Properties

Property	Test Method	E-50SM	E-75SM	E-100SM	E-200SM	E-100CM
Physical Properties						
Top Surface		1 mil Aluminized Polyester				1 mil Clear Polyester
Thickness		0.50	0.75	1.0	2.0	1.0
Density Nominal (lb./ft.³)	ASTM D3574	2.0	2.0	2.0	2.0	2.0
Weight Nominal (lb./ft.²)	ASTM D3574	.08	.13	.17	.35	.17
Flame	UL 94H	Meets HBF	Meets HBF	Meets HBF	Meets HBF	Meets HBF
	MVSS 302	Passes	Passes	Passes	Passes	Passes
	FAR 25.853 (b)					
	SAE J369 (a)					
Random Incidence Acoustical Absorption Coefficient	ASTM C423-84a and ASTM E795-83 (Mounting A) @ 125 Hz	0.11	0.12	0.20	0.50	0.17
	@ 250 Hz	0.08	0.30	0.81	0.62	0.74
	@ 500 Hz	0.60	0.67	0.61	0.91	0.63
	@1000 Hz	0.67	0.81	0.73	0.86	0.78
	@2000 Hz	0.87	0.77	0.71	0.75	0.69
	@4000 Hz	0.73	0.78	0.69	0.73	0.73
	NRC	0.55	0.65	0.70	0.80	0.70
Thermal Conductivity (K) (BTU-in./hr.-ft.²-deg.F)	ASTM C177			0.28		0.28
Thermal Resistivity (R) (hr.-ft.²-deg.F/BTU)	ASTM C177 *Calculated from 1-in. foam value	1.8*	2.7*	3.8	7.1*	3.8
Strength Properties						
Tensile Strength	ASTM D3574 Foam: lb. @ 23°C, ambient humidity Foam: lb. @ 70°C, 100% humidity x 2 wk. Foam: lb. @ 100°C, 100% humidity x 2 wk. Facing: lb.	38	38	19 18 15 36	36	19 18 15 17
Tear Strength	ASTM D3574 Foam: lb./in. Facing: lb./in. @ 1-in. width	0.6	0.6	3.0 0.6	0.6	3.0 0.7
Elongation* *Foam only	ASTM D3574 % @ room temp., ambient humidity % @ 70°C, 100% humidity x 2 wk. % @ 100°C, 100% humidity x 2 wk.			286 350 262		286 350 262
Compression Set	ASTM D3574 (% of original height @ 50% initial deflection, 70°C for 22 hr.)			18		18
Compression-Deflection	ASTM D3574, @ 50% Compression @ room temp., ambient humidity, psi @ 70°C, 100% humidity x 2 wk., psi @ 100°C, 100% humidity x 2 wk., psi			0.52 0.65 0.68		0.53 0.67 0.87

Figure 27 – Physical properties of acoustic foams provided by EAR Specialty Composites. Foam E-200SM was selected to be used as a wall lining on tunnel ducts. Figure is presented again in Appendix A14.

Fan noise will be attenuated with the use of a number of different countermeasures working in parallel. The first of these is the use of a honeycomb core (Figure 14, Section H) as a flow straightener immediately upstream of the fan inlet. It is anticipated that the flow straightener will reflect some pressure disturbances while dampening others through viscous effects occurring within each of the core cells.

The second fan noise countermeasure implemented is the plenum section upstream of the flow straightener. The plenum will dissipate noise emanating from the fan with a combination of reduced flow velocity and surrounding static fluid. Since pressure differentials are a function of velocity squared for flow along streamlines, velocity through the plenum section was kept as low as possible. It is also planned that noise propagating into the plenum will reflect off of its walls through static fluid where the noise will be dissipated through viscous effects.

Reflection of sound from the plenum walls will be minimized with installation of acoustic foam linings. The foam has Noise Reduction Coefficient (NRC) of 0.80, which means that only about 20% of sound energy in the frequency range of 125-4000 Hz will be reflected.

Fan noise is further stricken from entering the test section by the sudden expansion (sudden contraction with respect to the upstream direction) located at Station 5. With area ratio of 8.6 between Sections E and F, it is a safe assumption that only about 14% of noise existing within the plenum (Section F) will propagate into the diffuser. This noise will be further attenuated within the diffuser by the acoustic foam that will line its walls also.

That last countermeasure employed to attenuate fan noise is designing the tunnel so that the noise must propagate upstream. In comparison of experimental results published by Meyer & Neumann (1972) and shown in Figures 12 and 13, it is apparent that noise attenuation at duct walls is more effective when sound propagates opposite the direction of flow. With this, and all other means of attenuating fan noise working

together, it is doubtful any fan noise will propagate into the test section. And, attenuation of test section noise may be considered in absence of fan noise.

Attenuation of noise within the test section is to be performed with the acoustic foam lining on two adjacent walls. It is ideal to have the lining on all four walls, but fluid mechanics and instrumentation considerations restricted application of the foam to two walls. Foam was not specified to be applied to the wall that possessed the cavity nor one of its adjacent walls. It was speculated variations in foam thickness would exist in the sheet stock and that the variations would cause boundary layer management on the wall possessing the cavity to be difficult. Unsteady pressure measurement and the use of static pressure wall taps also required the wall to be rigid. The adjacent wall had to be transparent to accommodate PIV.

3.3 Instrumentation Considerations

This section discusses all features that were added to the quiet wind tunnel in order to accommodate necessary measurement instrumentation. The tunnel will be equipped with a total pressure, unsteady pressure, and instantaneous velocity field measurement systems.

3.3.1 Total Pressure Measurement

It is necessary that the wind tunnel possess a total pressure measurement system in order to calibrate the fan controller and to measure boundary layer characteristic thicknesses. Total pressure measurement is performed with a traversable pitot tube, static pressure wall tap, and pressure transducer. The total pressure measurement system needs to be implemented prior to experimentation with cavity flow since the pitot tube disturbs the flow. Implementing the system prior to experimentation allows for test section velocity and boundary layer characteristics to be determined as a function of fan speed.

To accommodate dynamic velocity profile measurement, a pressure transducer will connect both static and dynamic pressure ports and the pitot tube will be outfitted with both a screw drive mechanical traversing mechanism and LVDT. The combination of pitot tube and static wall tap are implemented at the same axial location in the test section as the cavity. The hardware is attached to a removable partition of test section wall. After the system is calibrated, an identical partition containing the side branch cavity can then be installed in its place.

3.3.2 Unsteady Pressure Measurement

Unsteady pressure measurement is necessary to resolve acoustic resonance. The measurement system consists of six static pressure wall taps bored into the rigid test

section wall that contains the cavity. Each of the wall taps is outfitted with microphone level pressure transducers capable of resolving pressures of 0.001 psi. Five of the wall taps are positioned upstream and inline with the center of the cavity. The sixth wall tap is positioned downstream and inline with the center of the cavity.

3.3.3 Instantaneous Velocity Field Measurement

Instantaneous velocity field measurement will be performed with the use of one of the PIV systems already existing in the Fluid Mechanics Research Laboratory. To accommodate a PIV system, the tunnel test section had to allow projection of laser light normal to the cavity mouth and camera imaging perpendicular to the laser illumination.

Familiarity with PIV systems allows the thickness of the illuminated laser sheet to be estimated to be less than a millimeter. A slit with thickness of 1/4 inch was specified to be placed along the center of the foam liner that was attached to the wall opposite the cavity to allow projection of the laser sheet into the test section. A transparent section of wall material was also implemented to allow transmission of laser light. The added width of the foam slit makes alignment of the laser easier for the experimentalist. A slit of 1/4 inch was determined to be the limit for preventing the introduction of sound attenuation deficiencies and disruption of the test flow.

The wall receiving the laser window was also specified to be at the bottom of the test section to accommodate laser traversing mechanisms already in use for the PIV

systems. This means that the wall possessing the cavity was oriented to be the upper or top wall of the test section. One of the side walls of the test section was specified to be transparent in order to accommodate digital imaging.

3.3.4 Measurement Sensitivity and Resolution

All of the measurement equipment specified for use in the quiet tunnel has been implemented in similar facilities used to study flow-acoustic coupling and has already demonstrated its effectiveness. It is worthwhile, however, to mention the minimum requirements for the tunnel.

The total pressure measurement system needs to resolve tunnel velocity to at least 1 fps. This requires a manometer with 14 inches of water capacity to measure velocities up to 250 fps and graduation of 0.000225 inches of water to resolve velocities of 1 fps. Replacing the manometer with a pressure transducer is desirable for this application. However, a sequence of manometers with low density measurement oil will be necessary for calibrating the transducer.

The system should also be capable of measuring velocity at 10 radial stations within the boundary layer. This means that the pitot tube must be capable of traversing through the boundary layer thicknesses at a minimum of 10 increments. Assuming a velocity of 250 fps (maximum test section velocity), boundary layer thickness, given by equation (10), at $x = 4$ ft. will be 0.097 inches, which means the pitot tube must traverse

at 0.010 inch increments. Likewise, for velocity of 18.8 fps (corresponds to 0.5 cfm flow rate through fan), boundary layer thickness at the same axial location will be 0.352 inches, which means the pitot tube must traverse at 0.035 inch increments. The pitot tube must therefore be capable of traversing through 0 to 0.352 inches at 0.010 inch increments.

Based on the assessment presented in Section 3.2.2, the unsteady pressure measurement system must be capable of resolving frequencies up to 2600 Hz. In order to resolve waveforms at this frequency, sampling rates of 26,000 Hz are necessary. Figure 6 shows that a typical flow acoustic resonance peaks at 0.010 psi. Transducer sensitivity necessary to resolve this amplitude should be a minimum of 0.001 psi. Filtering transducer signals above 2600 Hz is also appropriate to reduce the number of samples required to identify resonant frequencies with Fast Fourier Transform averaging.

3.4 Structural Considerations

This section addresses design considerations made for manufacture, assembly, and function of the quiet wind tunnel. Considerations made in choosing an appropriate material to construct the tunnel with are also presented.

3.4.1 Design for Manufacture

Design for manufacture involves choosing tunnel part geometry, dimensions, and tolerances so that the parts can be quickly and easily cut on in-house machines. It also involves communicating how to shape tunnel parts to in-house machinists. Much of the dimensioning and tolerancing work was automated with IDEAS computer aided engineering software. All the tunnels parts were modeled and assembled in a CAD database. After specifying appropriate datums, the IDEAS software generated paper drawings of tunnel parts complete with orthogonal and isometric view, dimensions, and tolerances.

Familiarity with in-house machines was also a major influence in choosing between the use of an acoustic foam and a rock wool and perforated sheet wall liner. The acoustic foam can be cut from its stock sheet to rough size with a jig saw and serrated blade. Finishing cuts can be performed on a band saw equipped with a serrated blade. The foam sections could then be quickly and easily applied to duct walls with a pressure sensitive adhesive.

It was estimated that constructing wall liners from perforated sheet would occupy as much as 10 times the manufacturing time as would cutting and applying the acoustic foam. Perforated sheet metal sections would need to be cut in a manner similar to the foam sections, but at a much slower rate. Also adding to the manufacturing time is the fabrication of members that would be required to maintain flatness of the sheet, bending operations that would be necessary to make the steel sheet conform to inlet contraction

curvature, and joining processes to attach one perforated sheet wall to another in order to prevent vibration.

3.4.2 Design for Assembly

The tunnel layout includes many features that add complexity to the manufacturing task, but were necessary for ease of assembly. One of these features is the development of section flanges. Flanges are necessary to permit sections to be constructed individually then connected once completed. Flanges were designed for both ends of the test section and diffuser.

The top and the transparent walls of the test section were designed so that they could be removed from the test section without having to disconnect the test section from the inlet contraction and plenum. This is an important feature that is necessary for applying tape to the joint of acoustic foam between the test section and the diffuser.

Another tunnel feature that was incorporated into design for assembly of the tunnel is the orientation of section walls. Because the material chosen to construct the tunnel with has high density and low elasticity, care was given not to create regions of concentrated stress in the wall material. This involved orienting all section walls so that the side walls rested atop the bottom wall and that the top wall rested atop the side walls. Only with such an orientation does all of the thickness of the bottom wall carry the load

imposed by the weight of the other walls. And the top wall uses all of its thickness to carry the load imposed by its own weight.

3.4.3 Design for Function

The tunnel also possesses features that make using it easy to conduct experiments. For example, the test section was designed so that laser projection for PIV would be performed from underneath it. This feature makes use of one of the laser traversing rigs that already exist in the laboratory. Orienting the test section walls so that laser projection would occur from the top or side of the test section would have required purchase or construction of additional hardware.

The test section also features removable wall sections that permit quick changing of cavity and/or total pressure measurement systems and cleaning of excess PIV oil in the test section. Incorporation of this feature prevents the need to remove the entire test section in order to clean or modify it. This would be a cumbersome task considering that the weight of the assembled test section is estimated to be in excess of 54 lbs.

The permeable baffles that are positioned within the plenum section also require periodic cleaning. This section of the tunnel has been designed so that the baffles may be quickly removed and installed. The filters are loaded into frames that slide in and out of the plenum section from the side. The frames are constructed from 1 inch aluminum U-channel and possess broad handles for ease of operation and aesthetics.

3.4.4 – Material Selection

The material chosen to fabricate the quiet tunnel with is an black acrylic plastic. This material was chosen since it has been implemented in most of the other experimental facilities within the laboratory. It was desirable to give the quiet tunnel the same look as the others.

Assurance that the material was a practical choice for use in fabricating the tunnel was gained by assessing the deflection and bending stress the test section walls would sustain. The test section is the only section that will not be supported directly. It is also the only section in which only two walls will carry the load of all four. (The wall possessing the cavity and an adjacent wall are both removable.)

The 1/2 inch acrylic plastic chosen to fabricate the tunnel with is manufactured by Plastiglas de Mexico (www.chemcastacrylic.com). It possesses 9.6 ksi tensile strength, 18 ksi compressive strength, 425 ksi elastic modulus, and 1.18 specific gravity. Using these properties, deflection of the test section was determined to be 0.0032 inches and bending stress was computed to be 0.14% of the tensile strength of the material and 0.2% of its compressive strength. It was therefore concluded that the material is practical for fabrication of tunnel sections.

4 – CONCLUSIONS AND RECOMMENDATIONS

Before concluding this work, there are a number of additional items that need to be addressed. First, it is difficult to speculate on the attenuation performance of the quiet tunnel. Attenuation performance was assessed in the Meyer & Neumann (1972) experiments by comparing pressure spectrum data obtained from tunnel test sections both with and without the acoustically absorbent liner. It is unclear whether suction fan noise attenuation was present in both cases. To assess the attenuation performance of the subject tunnel, it is proposed that a rigid wall test section be fabricated and installed in place of the test section lined with acoustically absorbent foam. The attenuation performance of the quiet section would then be the difference between pressure spectrums obtained from the quiet and rigid wall sections.

The height by which the side branch cavity protrudes into the test section flow should be variable. By making the cavity protrude into the test section flow, the experimentalist can effectively vary boundary layer characteristic lengths without altering test section velocity. Zero characteristic thicknesses can also be explored.

Back in Section 3.1.2, it was mention that press fitting honeycomb core so that it over expands to fill frames at Sections B and H is desirable to prevent vibration. It is important to note the expansion direction of the core before cutting it to size. Figure 28 illustrates both the expansion and ribbon directions.

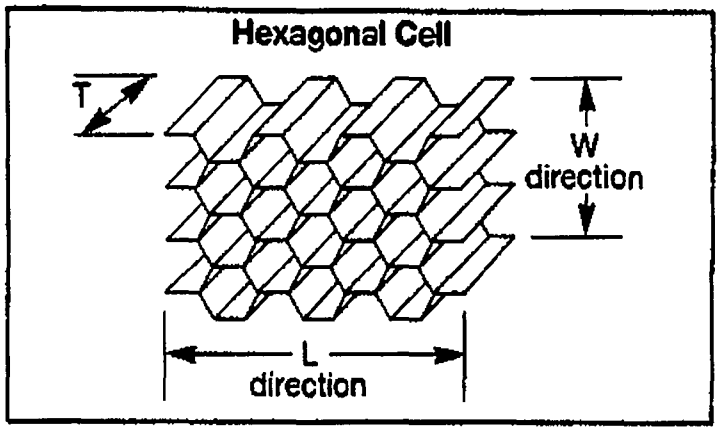

Figure 28 – Illustration of honeycomb core characteristic directions. W is the expansion direction, L is the ribbon direction.

In order to fit tightly into frames prepared at Sections B and H, the honeycomb core should be cut so that it is 1/4 inch shy of the target dimension in the expansion direction and 1/4 inch over the target dimension in the ribbon direction. Compression in the ribbon direction will then cause over expansion of the core so that it fills the square frames at Sections B and H. Because the core is formed from 0.0015 inch aluminum ribbon, it is recommended that gloves be worn when pressing the core into the frames.

5 – REFERENCES

Adrian, R.J., Christensen, K. T., and Liu, Z. C. 2000. *Analysis and Interpretation of Instantaneous Turbulent Velocity Fields.* Experiments In Fluids. Vol.29, p.275-290.

Adrian, R.J., 1991. *Particle-Imaging Techniques for Experimental Fluid Mechanics.* Annual Review of Fluid Mechanics. Vol.23, p.261-304.

Adrian, R.J., 1986. *Multi-Point Optical Measurements of Simultaneous Vectors in Unsteady Flow – A Review.* International Journal of Heat and Fluid Flow. Vol.7, No.2. June.

Barna, P.S., 1996. *Results of Tests Performed on the Acoustic Quiet Flow Facility Three-Dimensional Model Tunnel – Final Report on the Modified D.S.M.A Design.* NASA Contractor Report No.198312. Langley Research Center, Hampton, Virginia.

Barna, P.S., 1995. *Results of Tests Performed on the Acoustic Quiet Flow Facility Three-Dimensional Model Tunnel – Progress Report on the Modified D.S.M.A Design.* NASA Contractor Report No.198311. Langley Research Center, Hampton, Virginia.

Blake, W.K., 1986. *Mechanics of Flow-Induced Sound and Vibration, Vols. 1 and 2,* New York Academic Press.

Fox, R.W., and McDonald, A.T., 1998. *Introduction to Fluid Mechanics, 5^{th} ed.* John Wiley & Sons, New York.

Hall, D.G. and Woodward, R.P., 1996. *Assessment of Noise Control Measures for a Model Advance Ducted Propulsor*. Journal of Aircraft, Vol.33, No.3, p.505-510.

Howe, M.S., 1997. *Edge, Cavity and Aperture Tones at Very Low Mach Numbers*. Journal of Fluid Mechanics, Vol.330, p.61-84.

Meyer, E. and Neumann, E. G., 1972. *Physical and Applied Acoustics*. Academic Press, London, Ch.11.2, p.399.

Mosher, M., 1992. *Evaluation of Discrete Frequency Sound in Closed-Test-Section Wind Tunnels*. Journal of Aircraft, Vol.29, No.5, p.753-759.

Karadogan, H. and Rockwell, D., 1983. *Toward Attenuation of Self-Sustained Oscillation of a Turbulent Jet Through a Cavity*. Journal of Fluids Engineering, Vol.105, p.335-340.

Knisely C. and Rockwell, D. 1982. *Self-Sustained Low-Frequency Components in an Impinging Shear Layer*. Journal of Fluid Mechanics, Vol.116, p.157-186.

Rockwell, D., 2000. *Flow-Acoustic Coupling of a Side Branch Resonator*. Proposal to Perform Scientific Research, Lehigh University Department of Mechanical Engineering, Bethlehem, Pennsylvania.

Rockwell, D., 1983. *Oscillations of Impinging Shear Layers.* Invited Lecture, 20th Aerospace Sciences Meeting of AIAA, January, 1981, Orlando, FL; AIAA Paper 81-0047; also see AIAA Journal, Vol.21, p.645-664.

Rockwell, D., 1998. *Vortex-Body Interactions.* Invited contribution to Annual Review of Fluid Mechanics, Vol.30, p.199-229.

Rockwell, D. and Naudascher, E., 1979. *Self-Sustained Oscillations of Impinging Free Shear Layers.* Annual Review of Fluid Mechanics, Vol.11, p.67-94.

Rockwell, D. and Naudascher, E., 1978. *Review – Self-Sustained Oscillations of Flow Past Cavities.* Transactions of the ASME, Vol.100, p.152-165.

Rockwell, D. and Schachenmann, A., 1982. *Self-Generation of Organized Waves in an Impinging Turbulent Jet at Low Mach Numbers.* Journal of Fluid Mechanics, Vol.117, p.425-441.

Rockwell, D. and Schachenmann, A., 1983. *The Organized Shear Layer due to Oscillations of a Turbulent Jet Through an Axisymmetric cavity.* Journal of Sound and Vibration, Vol. 87, p.371-382.

Runstadler, P.W., Jr., Dolan, F.X., and Dean, R.C., Jr. 1975. *Diffuser Data Book*. Creare Inc., Hanover, NH, Technical Note 186.

Schmitz, F.H., Boxwell, D.A., Splettstoesser, W.R., Schultz, K.J., Lewy, S., and Caplot, M., 2000. *Model Helicopter Rotor Aerodynamics and Acoustics As Measured in Two Anechoic Wind Tunnels*. Journal of Aircraft, Vol.37, No.2, p.235-244.

Schneider, S.P. and Haven, C.E., 1995. *Quiet-Flow Ludwieg Tube for High-Speed Transition Research*. AIAA Journal, Vol.33, No.4, p.688-693.

Sivian, L.J, 1937. Sound Propagation in Ducts Lined with Absorbing Materials. Journal of the Acoustical Society of America, Volume 9, p.135-140.

Vincent, C., 2000. *Attenuation of Flow-Acoustic Coupling with Passive Vortex Generator*. Undergraduate Research Project Report. Lehigh University Department of Mechanical Engineering, Bethlehem, Pennsylvania.

Woodward, R.P., Bock, L.A., Heidelberg, L.J., and Hall, D.G., 1994. *Model Ducted Propulsor Noise Characteristics at Takeoff Conditions*. Journal of Aircraft, Vol.31, No.5, p.1064-1070.

APPENDIX

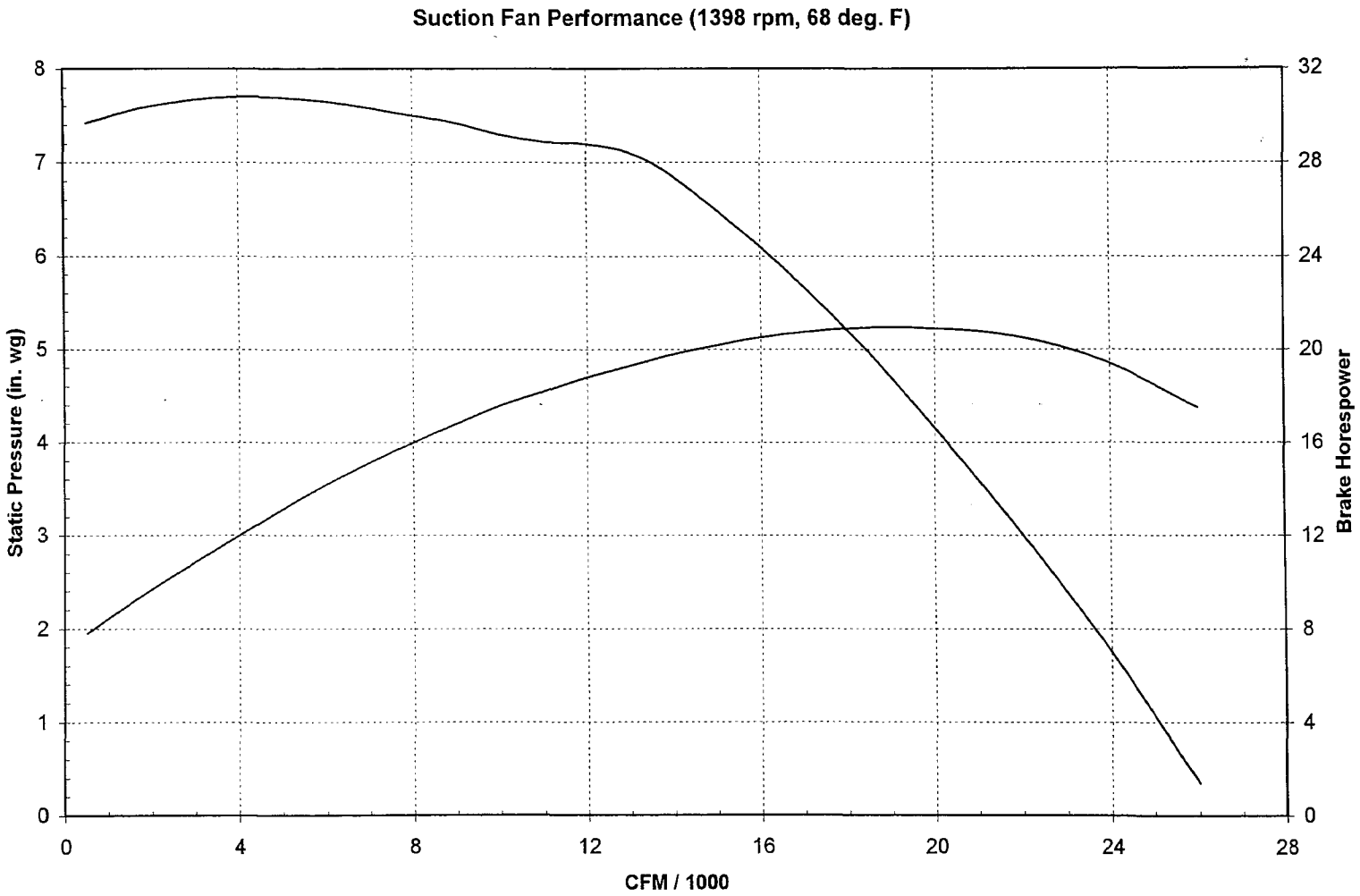

Appendix A1: Performance map for Twin City suction fan model 330 BAF-SW with operation at design conditions.

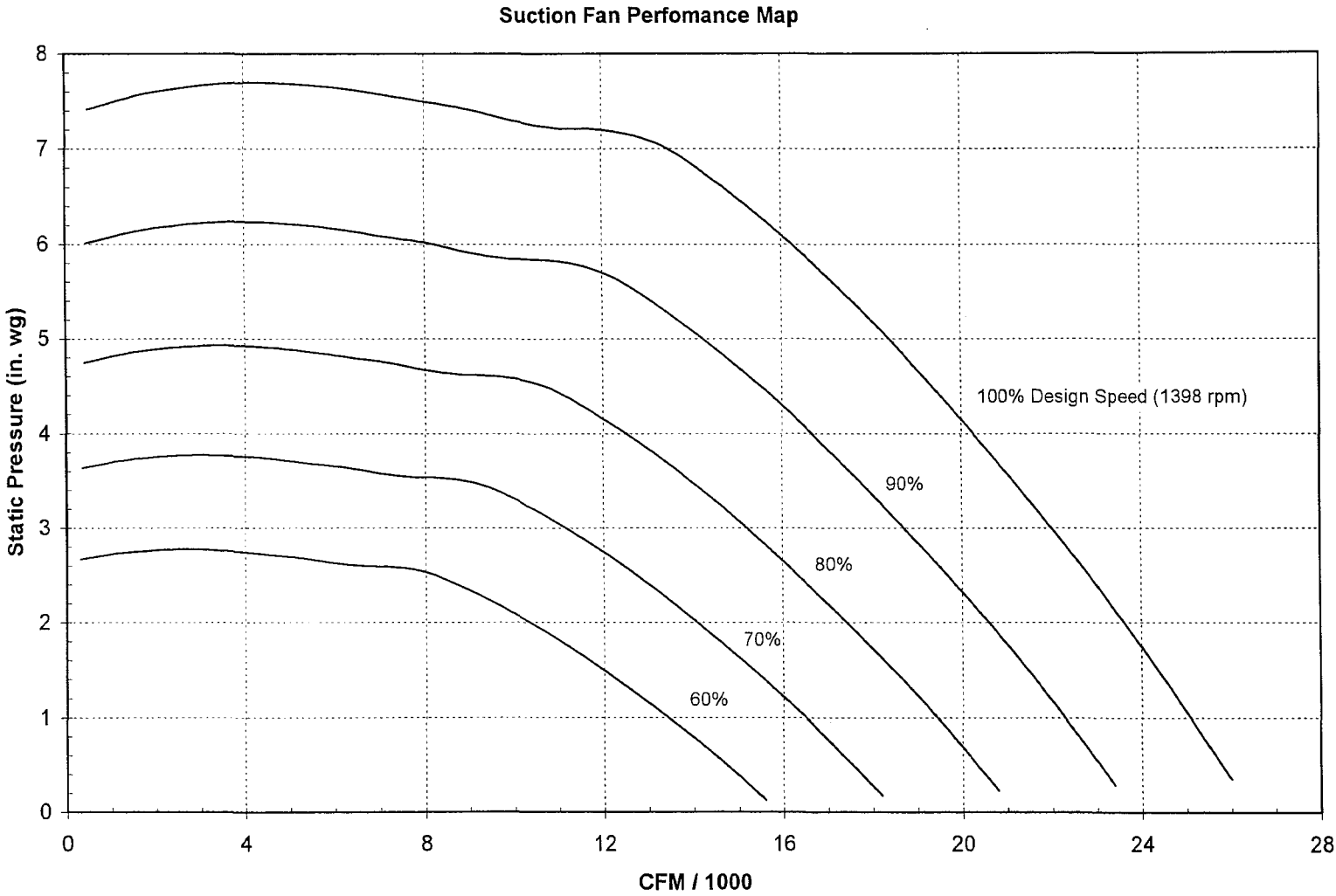

Appendix A2: Suction fan performance at 70, 80, 90, and 100 percent design speed (with 68 deg.F inlet air temperature).

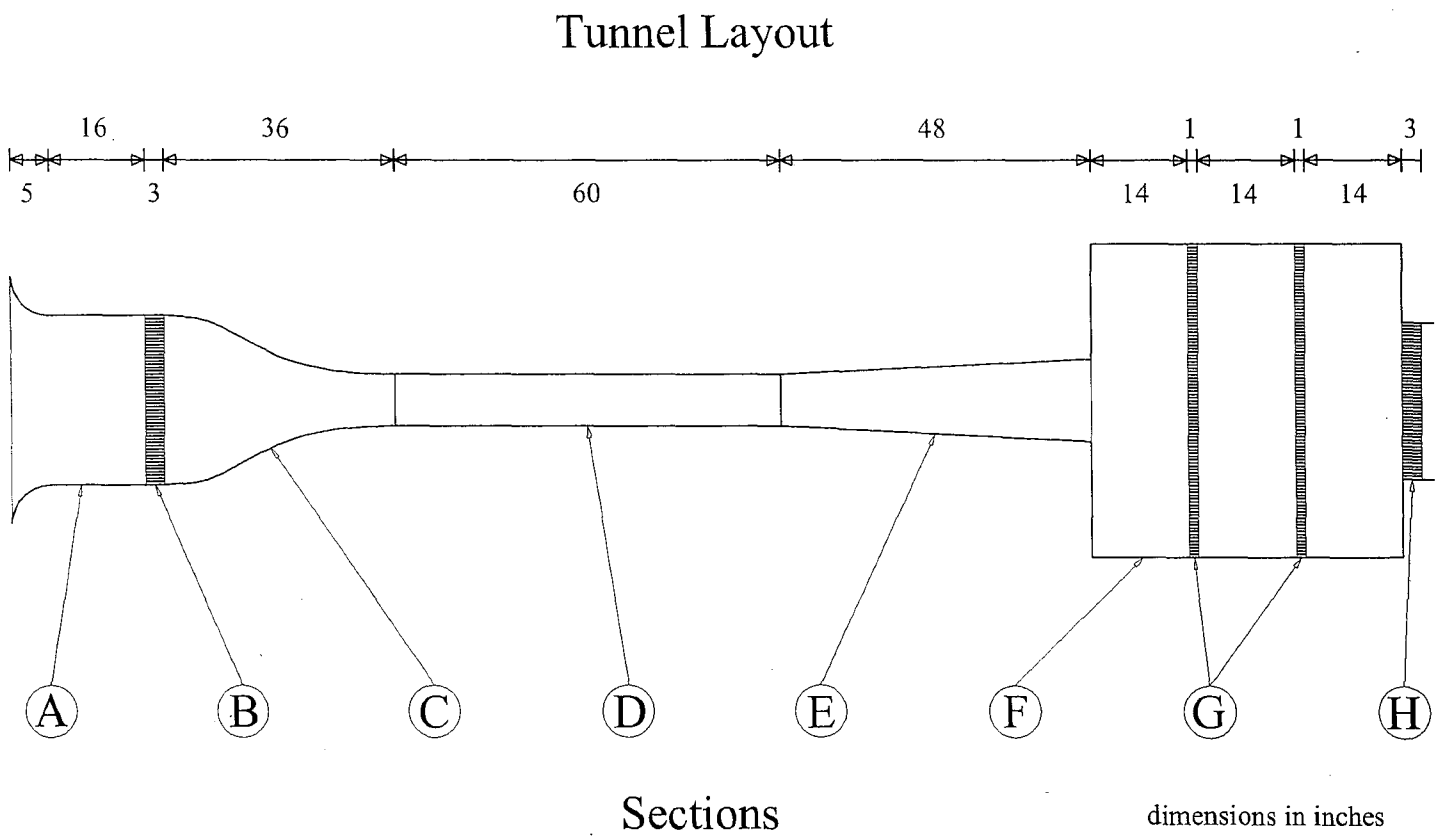

Appendix A3: Sketch of tunnel interior geometry shown with sections drawn to scale.

Table I: CR III 5052 Hexagonal Aluminum Honeycomb

Hexcel Honeycomb Designation Cell Size – Alloy – Foil Gauge	Nominal Density pcf	Compressive					Crush Strength psi	Plate Shear					
		Bare		Stabilized				L Direction			W Direction		
		Strength psi		Strength psi		Modulus ksi		Strength psi		Modulus ksi	Strength psi		Modulus ksi
		typ	min	typ	min	typ	typ	typ	min	typ	typ	min	typ
1/16 – 5052 – .0007@*	6.5	950	740	1000	780	275	505x	560	440	90.0	350	270	40.0
1/16 – 5052 – .001@*	9.2	1500	1170	1550	1200	420	750x	850	660	105.0	520	400	53.0
1/16 – 5052 – .0015@	12.4	2430	1900	2650	2000	650	1200x	1150	900	210.0	715	560	65.0
1/8 – 5052 – .0007	3.1	285	200	300	215	75	130	210	155	45.0	130	90	22.0
1/8 – 5052 – .001	4.5	550	375	570	405	150	260	340	285	70.0	220	168	31.0
1/8 – 5052 – .0015	6.1	980	650	1020	680	240	450	560	455	98.0	340	272	41.0
1/8 – 5052 – .002	8.1	1500	1000	1560	1100	350	750	800	670	135.0	470	400	54.0
1/8 – 5052 – .0025	10.0	2100p	1575p	2250p	1685p	–	–	980p	735p	175.0p	550p	415p	65.0p
1/8 – 5052 – .003@	12.0	2700	2100	2900	2200	900	–	1940I	1250I	–	1430I	1000I	–
5/32 – 5052 – .0007*	2.6	220	150	240	160	55	90	165	120	37.0	100	70	19.0
5/32 – 5052 – .001*	3.8	395	285	410	300	110	185	270	215	56.0	165	125	26.4
5/32 – 5052 – .0015*	5.3	690	490	720	535	195	340	420	370	84.0	270	215	36.0
5/32 – 5052 – .002*	6.9	1080	770	1130	800	285	575	590	540	114.0	375	328	46.4
5/32 – 5052 – .0025*	8.4	1530	1070	1600	1180	370	800	760	690	140.0	475	420	56.0
3/16 – 5052 – .0007*	2.0	160	90	175	100	34	60	120	80	27.0	70	46	14.3
3/16 – 5052 – .001	3.1	290	200	335	215	75	130	210	155	45.0	125	90	22.0
3/16 – 5052 – .0015	4.4	520	360	550	385	145	250	330	280	68.0	215	160	30.0
3/16 – 5052 – .002*	5.7	820	560	860	600	220	390	460	410	90.0	300	244	38.5
3/16 – 5052 – .0025*	6.9	1120	770	1175	800	285	575	590	540	114.0	375	328	46.4
3/16 – 5052 – .003*	8.1	1600	1000	1720	1100	350	750	725	670	135.0	480	400	54.0
1/4 – 5052 – .0007*	1.6	90	60	100	70	20	40	85	60	21.0	50	32	11.0
1/4 – 5052 – .001	2.3	190	120	210	130	45	75	140	100	32.0	85	57	16.2
1/4 – 5052 – .0015	3.4	340	240	370	250	90	150	230	180	50.0	140	105	24.0
1/4 – 5052 – .002	4.3	500	350	540	370	140	230	320	265	68.0	200	155	29.8
1/4 – 5052 – .0025	5.2	690	500	760	510	190	335	410	360	82.0	265	200	35.4
1/4 – 5052 – .003*	6.0	990	630	1100	660	235	430	530	445	96.0	340	265	40.5
1/4 – 5052 – .004	7.9	1420	970	1490	1050	340	725	700	650	130.0	440	390	52.8
3/8 – 5052 – .0007*	1.0	50	20	55	20	10	25	45	32	12.0	30	20	7.0
3/8 – 5052 – .001*	1.6	90	60	95	70	20	40	85	60	21.0	50	32	11.0
3/8 – 5052 – .0015*	2.3	190	120	200	130	45	75	135	100	32.0	80	57	16.2
3/8 – 5052 – .002*	3.0	285	190	310	200	70	120	200	145	43.0	125	85	21.2
3/8 – 5052 – .0025*	3.7	370	270	410	285	105	180	250	200	55.0	160	115	26.0
3/8 – 5052 – .003	4.2	520	335	560	355	135	220	310	255	65.0	200	150	29.0
3/8 – 5052 – .004	5.4	740	500	800	535	200	360	430	380	86.0	280	228	36.8
3/8 – 5052 – .005*	6.5	950	700	1000	750	265	505	545	500	105.0	350	300	43.5

Test data obtained at 0.625 inch thickness.

p = preliminary

x = predicted values

* Minimum block (48" x 96" x 30") purchase may be required.

I = Beam shear for 12.0 pcf products.

@ Maximum block size 42" x 60" for 1/8 – .003-12.0, all 1/16 cell size.

Appendix A4: Mechanical properties of Hexcel 5052 Aluminum Honeycomb core.

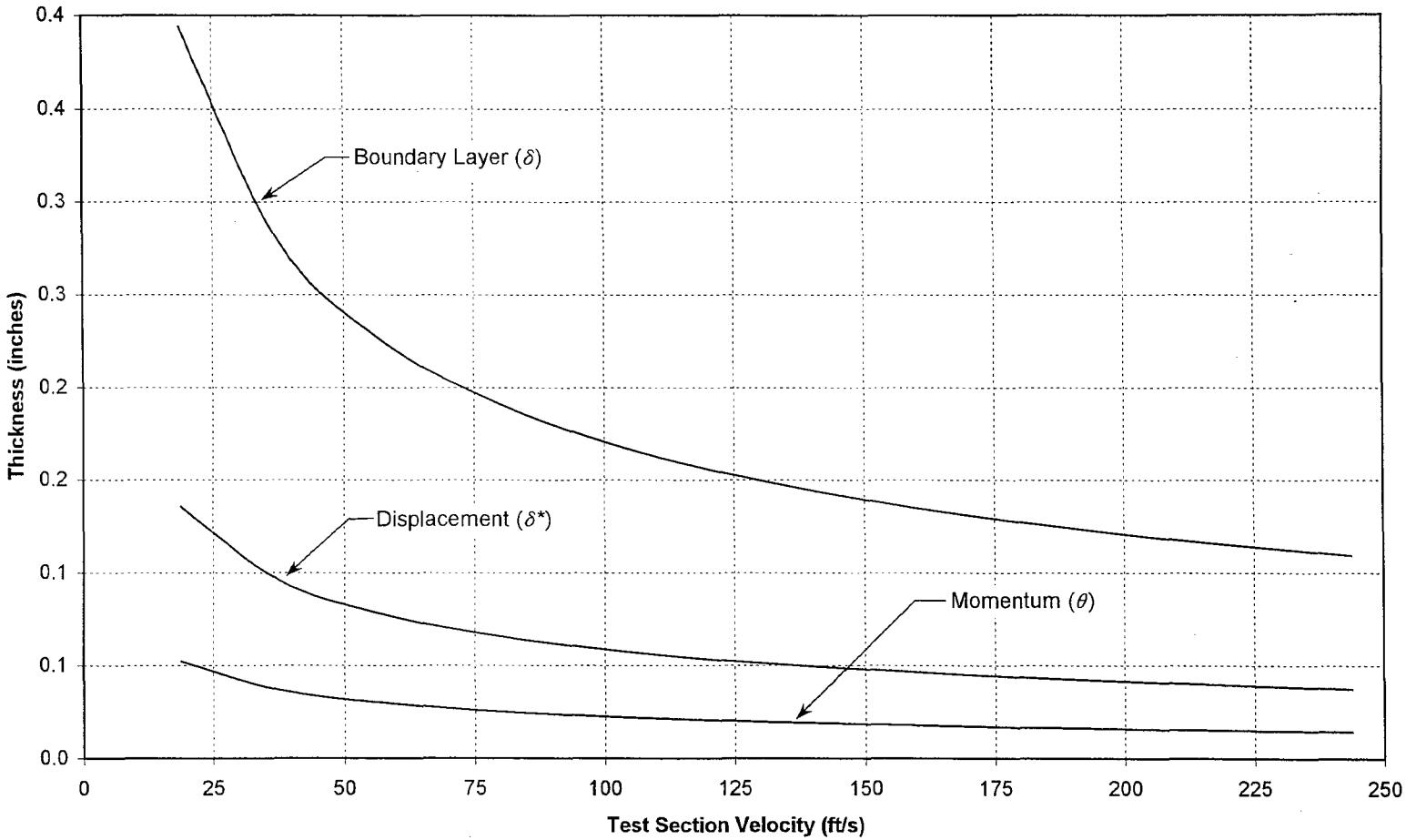

Appendix A5: Maximum boundary layer characteristic thicknesses projected to exist at test section outlet (thicknesses reflect zero pressure gradient)

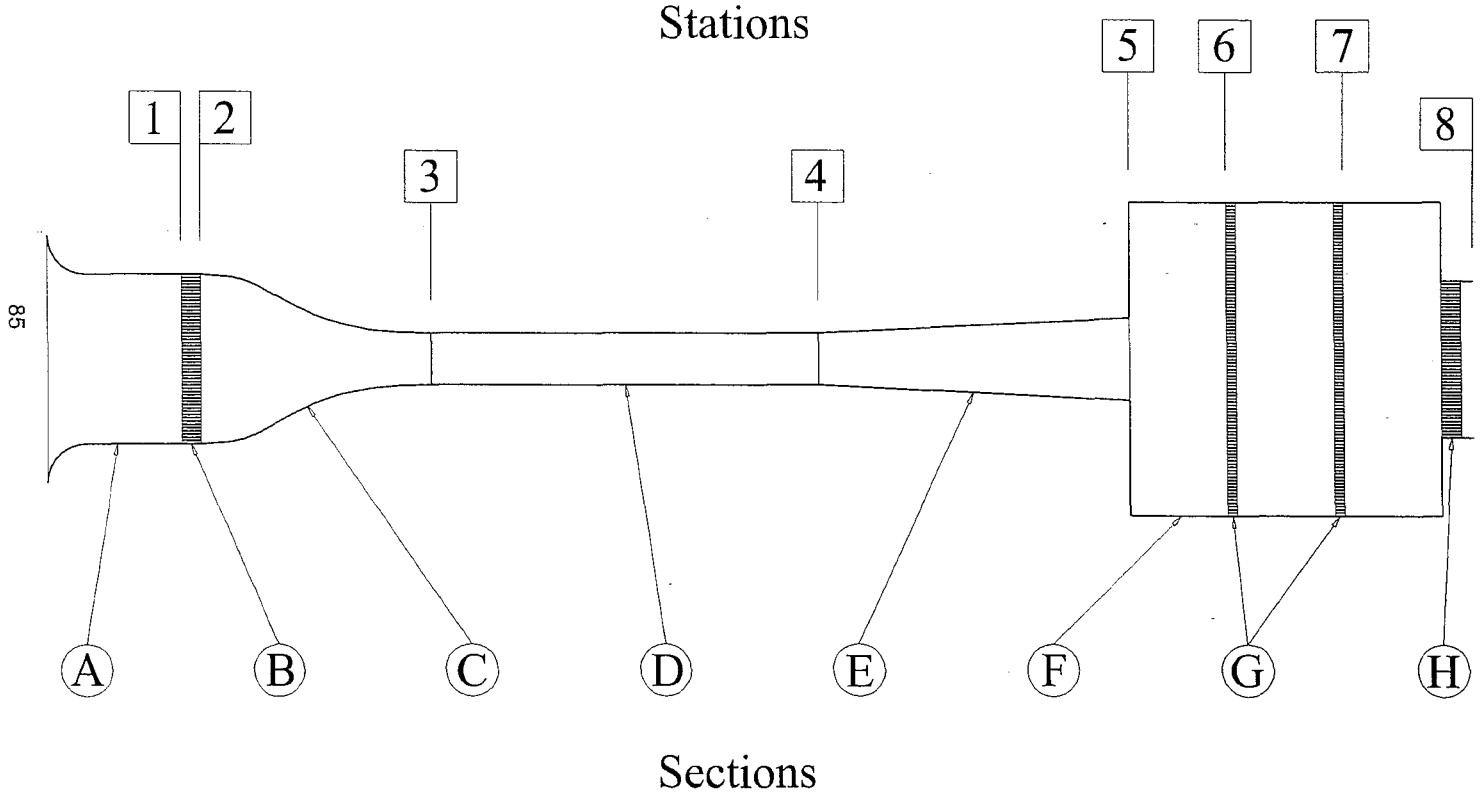

Appendix A6: Illustration of station assignment for calculation of total head.

Head Loss Through Aluminum Honeycomb Core

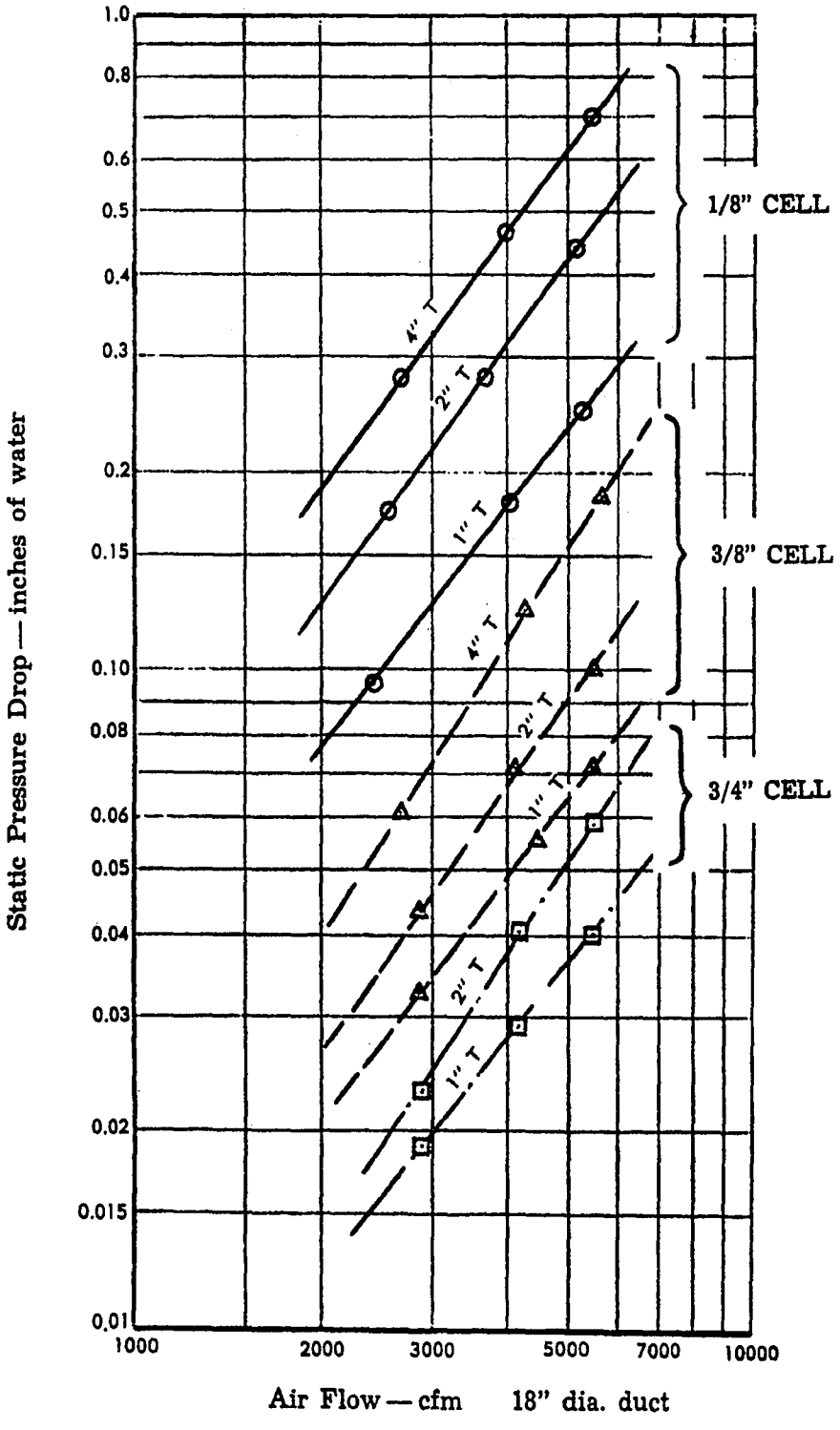

Appendix A7: Head loss data for aluminum honeycomb core of various cell sizes and thicknesses as a function of velocity (Hexcel).

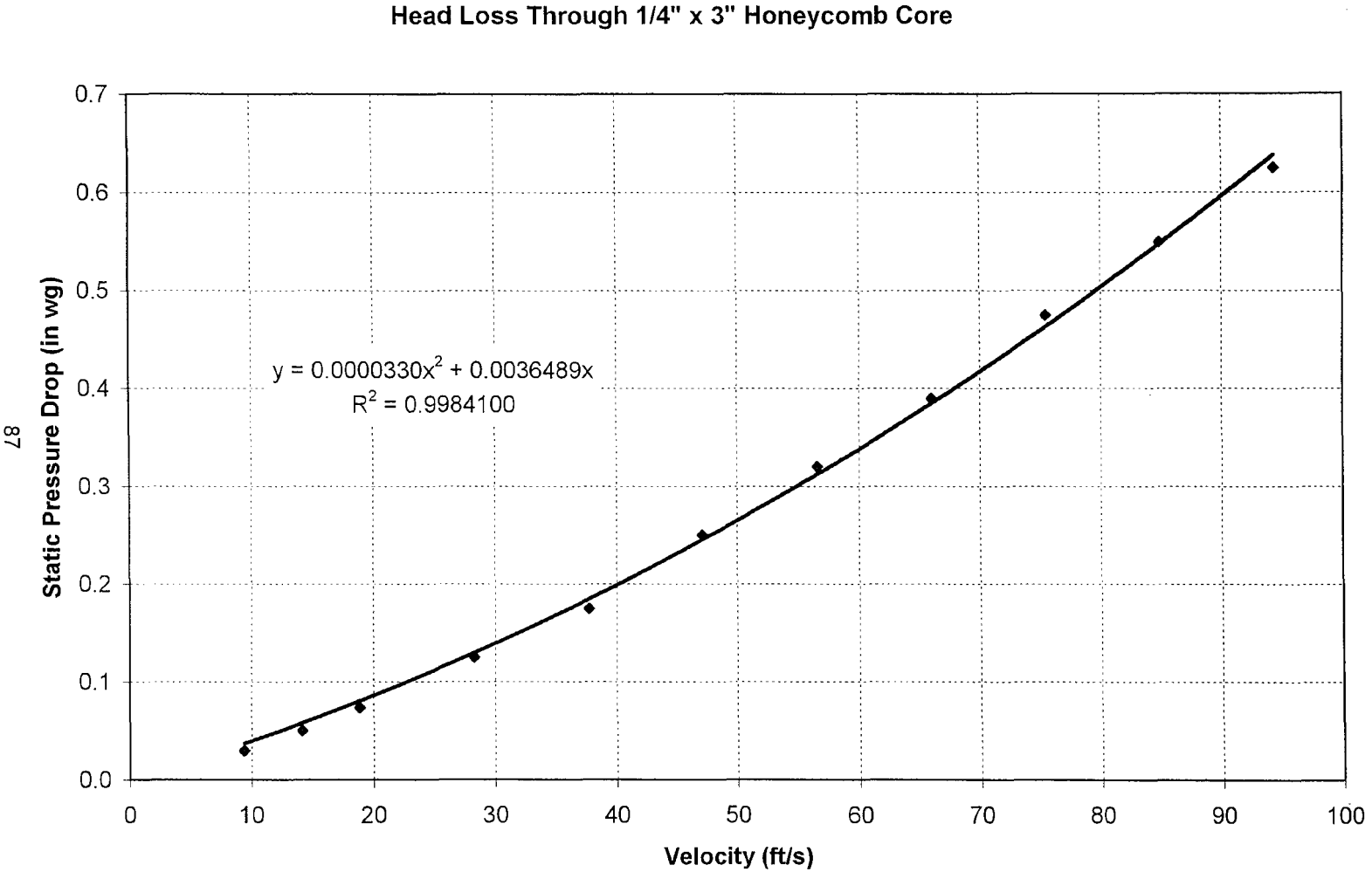

Appendix A8: Head loss characteristic for 1/4 x 3" honeycomb core interpolated from data presented in Appendix A7.

Moody Chart: Pipe Friction Factor as a Function of Reynolds Number

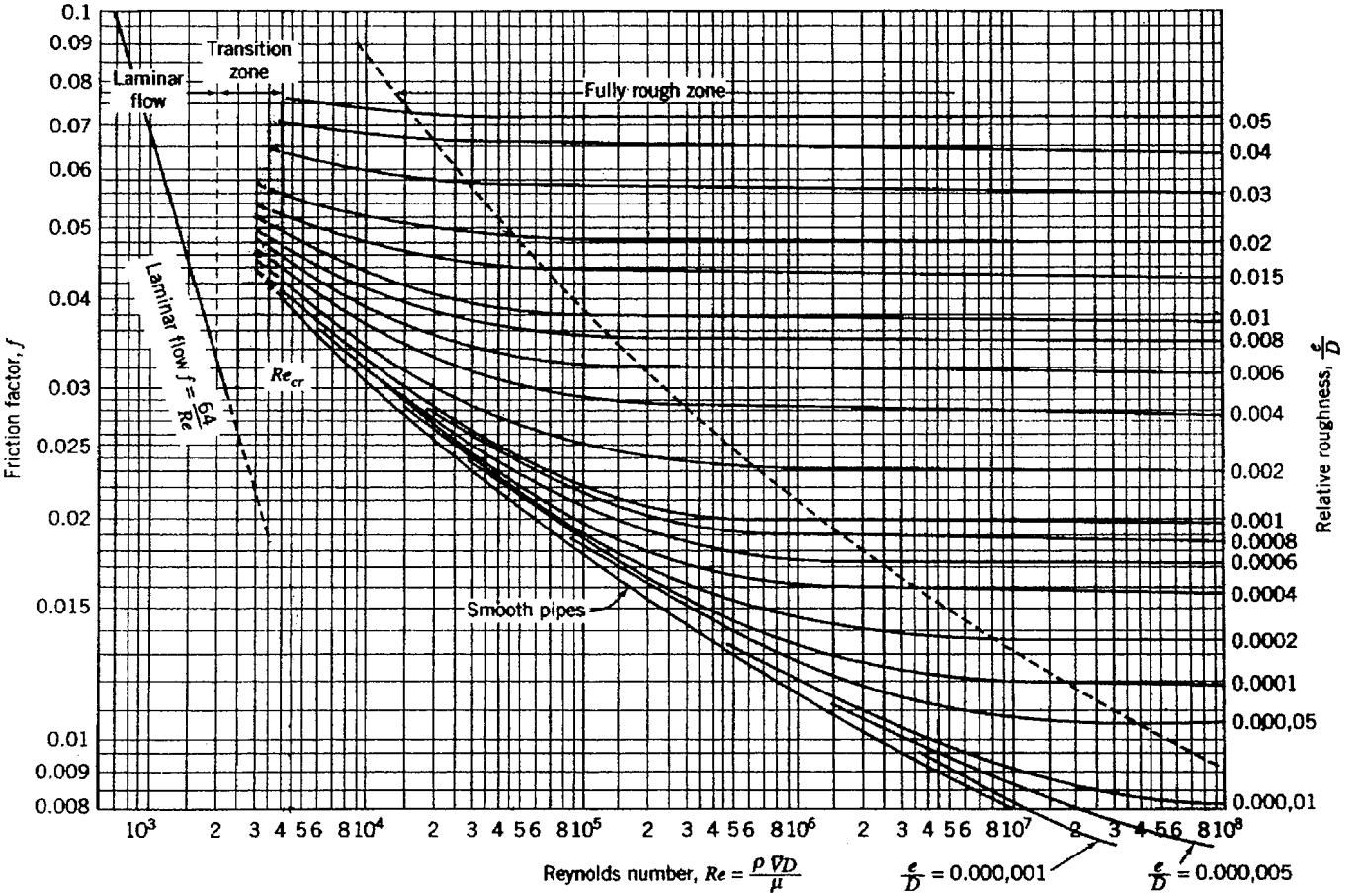

Appendix A9: Moody Chart for evaluation of duct friction losses as a function of Reynolds number (Fox & McDonald, 1998)

Pressure Recovery for Conical Diffusers

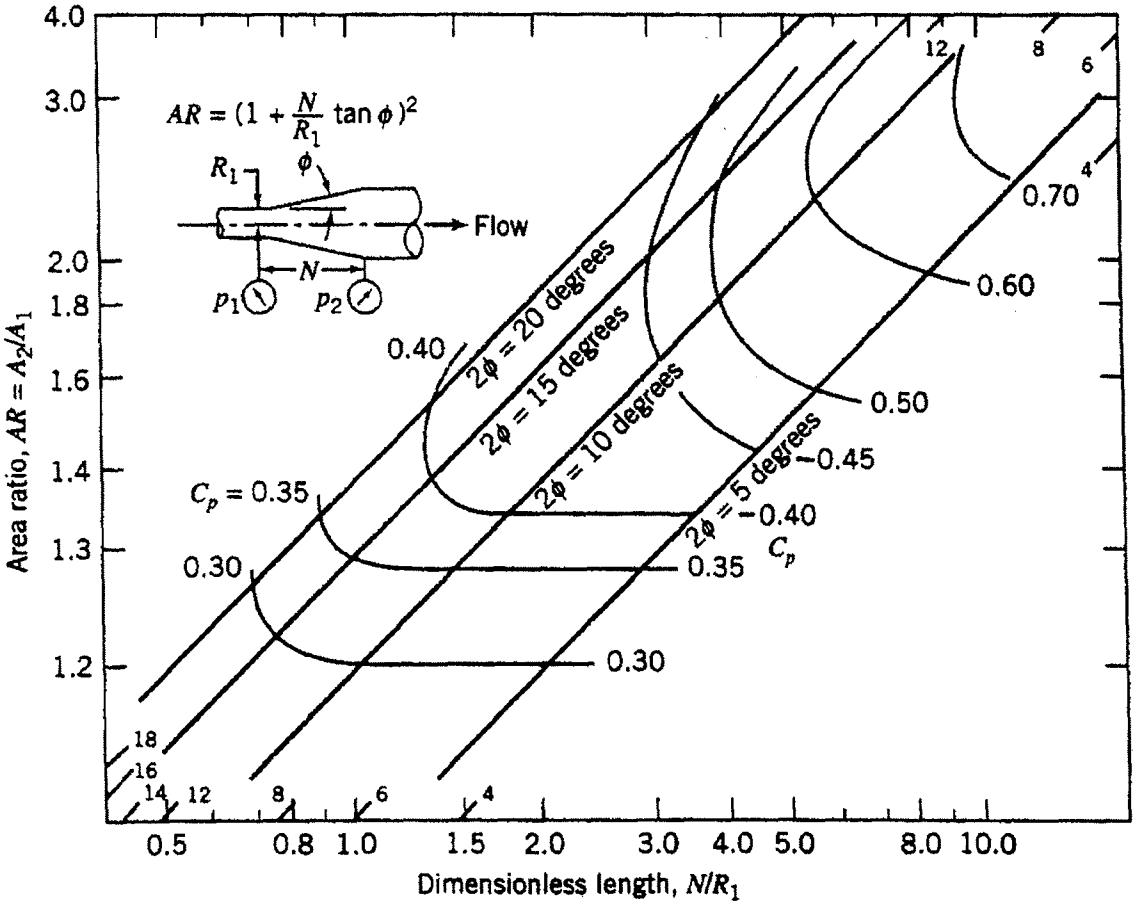

Appendix A10: Pressure recovery for conical diffuses with fully developed turbulent inlet flow (Runstadler et al., 1975 reprinted by Fox & McDonald, 1998).

AIR properties @ 68 deg. F

rho = 0.00234 slug/ft^3
mu = 3.79E-07 lbf*s/ft^2

WATER properties @ 68 deg F

rho = 1.94 slug/ft^3

Large area to small area --> negative static load
friction load ----> negative

V0 = 0
P0 = 0

Station 1 (before honeycomb) A = 4.694 ft^2
K = 0.04

Station 2 (after honeycomb) A = 4.694 ft^2

CFM (x 1000)		V1 (ft/s)	Static Load (in. wg)	Friction Load (in. wg)	Total Head (in. wg)	P1 (in wg)	V2 (ft/s)	Static Load (in. wg)	(Empirical) Friction Load (in. wg)	Total Head (in. wg)	P2 (in wg)
0.5		1.8	-0.001	0.000	-0.001	-0.001	1.8	0.000	-0.007	-0.007	-0.007
1.0		3.6	-0.003	0.000	-0.003	-0.003	3.6	0.000	-0.013	-0.013	-0.016
1.5		5.3	-0.006	0.000	-0.007	-0.007	5.3	0.000	-0.020	-0.020	-0.026
2.0		7.1	-0.011	0.000	-0.012	-0.012	7.1	0.000	-0.026	-0.026	-0.038
2.5		8.9	-0.018	-0.001	-0.018	-0.018	8.9	0.000	-0.033	-0.033	-0.051
3.0		10.7	-0.025	-0.001	-0.027	-0.027	10.7	0.000	-0.039	-0.039	-0.066
3.5		12.4	-0.035	-0.001	-0.036	-0.036	12.4	0.000	-0.046	-0.046	-0.082
4.0	*	14.2	-0.045	-0.002	-0.047	-0.047	14.2	0.000	-0.052	-0.052	-0.099
4.5		16.0	-0.057	-0.002	-0.060	-0.060	16.0	0.000	-0.059	-0.059	-0.118
5.0		17.8	-0.071	-0.003	-0.074	-0.074	17.8	0.000	-0.065	-0.065	-0.139
5.5		19.5	-0.086	-0.003	-0.089	-0.089	19.5	0.000	-0.072	-0.072	-0.161
6.0		21.3	-0.102	-0.004	-0.106	-0.106	21.3	0.000	-0.078	-0.078	-0.184
6.5		23.1	-0.120	-0.005	-0.124	-0.124	23.1	0.000	-0.085	-0.085	-0.209
7.0		24.9	-0.139	-0.006	-0.144	-0.144	24.9	0.000	-0.092	-0.092	-0.236

Station 1 (before honeycomb) A = 4.694 ft^2
K = 0.04

Station 2 (after honeycomb) A = 4.694 ft^2

CFM (x 1000)		V1 (ft/s)	Static Load (in. wg)	Friction Load (in. wg)	Total Head (in. wg)	P1 (in wg)	V2 (ft/s)	Static Load (in. wg)	(Empirical) Friction Load (in. wg)	Total Head (in. wg)	P2 (in wg)
0.5		1.8	-0.001	0.000	-0.001	-0.001	1.8	0.000	-0.007	-0.007	-0.007
1.0		3.6	-0.003	0.000	-0.003	-0.003	3.6	0.000	-0.013	-0.013	-0.016
1.5		5.3	-0.006	0.000	-0.007	-0.007	5.3	0.000	-0.020	-0.020	-0.026
2.0		7.1	-0.011	0.000	-0.012	-0.012	7.1	0.000	-0.026	-0.026	-0.038
2.5		8.9	-0.018	-0.001	-0.018	-0.018	8.9	0.000	-0.033	-0.033	-0.051
3.0		10.7	-0.025	-0.001	-0.027	-0.027	10.7	0.000	-0.039	-0.039	-0.066
3.5		12.4	-0.035	-0.001	-0.036	-0.036	12.4	0.000	-0.046	-0.046	-0.082
4.0	*	14.2	-0.045	-0.002	-0.047	-0.047	14.2	0.000	-0.052	-0.052	-0.099
4.5		16.0	-0.057	-0.002	-0.060	-0.060	16.0	0.000	-0.059	-0.059	-0.118
5.0		17.8	-0.071	-0.003	-0.074	-0.074	17.8	0.000	-0.065	-0.065	-0.139
5.5		19.5	-0.086	-0.003	-0.089	-0.089	19.5	0.000	-0.072	-0.072	-0.161
6.0		21.3	-0.102	-0.004	-0.106	-0.106	21.3	0.000	-0.078	-0.078	-0.184
6.5		23.1	-0.120	-0.005	-0.124	-0.124	23.1	0.000	-0.085	-0.085	-0.209
7.0		24.9	-0.139	-0.006	-0.144	-0.144	24.9	0.000	-0.092	-0.092	-0.236
		(after honeycomb)		A =	1.767						

Appendix A11: Tabulated head loss and static load for tunnel components as a function of flow rate.

Station 3		A =	0.444	ft^2	Station 4		A =	0.444	ft^2		
(test section inlet)		K =	0.05		(diffuser inlet)						
	(rel. to P2)										
V3 (ft/s)	Static Load (in. wg)	Friction Load (in. wg)	Total Head (in. wg)	P3 (in wg)	V4 (ft/s)	Static Load (in. wg)	ReDh	f (moody)	Friction Load (in. wg)	Total Head (in. wg)	P4 (in wg)
18.8	-0.078	-0.004	-0.082	-0.090	18.8	0.000	7.7E+04	0.0188	-0.011	-0.011	-0.101
37.5	-0.313	-0.016	-0.329	-0.345	37.5	0.000	1.5E+05	0.0163	-0.039	-0.039	-0.384
56.3	-0.705	-0.036	-0.740	-0.767	56.3	0.000	2.3E+05	0.0152	-0.081	-0.081	-0.848
75.0	-1.253	-0.063	-1.316	-1.354	75.0	0.000	3.1E+05	0.0141	-0.134	-0.134	-1.488
93.8	-1.958	-0.099	-2.056	-2.108	93.8	0.000	3.9E+05	0.0135	-0.200	-0.200	-2.308
112.5	-2.819	-0.142	-2.961	-3.027	112.5	0.000	4.6E+05	0.0132	-0.282	-0.282	-3.309
131.3	-3.837	-0.194	-4.031	-4.112	131.3	0.000	5.4E+05	0.0128	-0.372	-0.372	-4.484
150.0	-5.012	-0.253	-5.265	-5.364	150.0	0.000	6.2E+05	0.0125	-0.474	-0.474	-5.838
168.8	-6.343	-0.320	-6.663	-6.781	168.8	0.000	6.9E+05	0.0123	-0.590	-0.590	-7.372
187.5	-7.831	-0.395	-8.226	-8.365	187.5	0.000	7.7E+05	0.0120	-0.711	-0.711	-9.076
206.3	-9.475	-0.478	-9.953	-10.114	206.3	0.000	8.5E+05	0.0118	-0.846	-0.846	-10.960
225.0	-11.276	-0.569	-11.845	-12.030	225.0	0.000	9.3E+05	0.0117	-0.998	-0.998	-13.028
243.8	-13.234	-0.668	-13.902	-14.111	243.8	0.000	1.0E+06	0.0115	-1.152	-1.152	-15.263
262.5	-15.348	-0.774	-16.123	-16.358	262.5	0.000	1.1E+06	0.0114	-1.324	-1.324	-17.683

Station 3		A =	0.444	ft^2	Station 4		A =	0.444	ft^2		
(test section inlet)		K =	0.05		(plenum inlet)						
	(rel. to P2)										
V3 (ft/s)	Static Load (in. wg)	Friction Load (in. wg)	Total Head (in. wg)	P3 (in wg)	V4 (ft/s)	Static Load (in. wg)	ReDh	f (moody)	Friction Load (in. wg)	Total Head (in. wg)	P4 (in wg)
18.8	-0.078	-0.004	-0.082	-0.090	18.8	0.000	7.7E+04	0.0188	-0.011	-0.011	-0.101
37.5	-0.313	-0.016	-0.329	-0.345	37.5	0.000	1.5E+05	0.0163	-0.039	-0.039	-0.384
56.3	-0.705	-0.036	-0.740	-0.767	56.3	0.000	2.3E+05	0.0152	-0.081	-0.081	-0.848
75.0	-1.253	-0.063	-1.316	-1.354	75.0	0.000	3.1E+05	0.0141	-0.134	-0.134	-1.488
93.8	-1.958	-0.099	-2.056	-2.108	93.8	0.000	3.9E+05	0.0135	-0.200	-0.200	-2.308
112.5	-2.819	-0.142	-2.961	-3.027	112.5	0.000	4.6E+05	0.0132	-0.282	-0.282	-3.309
131.3	-3.837	-0.194	-4.031	-4.112	131.3	0.000	5.4E+05	0.0128	-0.372	-0.372	-4.484
150.0	-5.012	-0.253	-5.265	-5.364	150.0	0.000	6.2E+05	0.0125	-0.474	-0.474	-5.838
168.8	-6.343	-0.320	-6.663	-6.781	168.8	0.000	6.9E+05	0.0123	-0.590	-0.590	-7.372
187.5	-7.831	-0.395	-8.226	-8.365	187.5	0.000	7.7E+05	0.0120	-0.711	-0.711	-9.076
206.3	-9.475	-0.478	-9.953	-10.114	206.3	0.000	8.5E+05	0.0118	-0.846	-0.846	-10.960
225.0	-11.276	-0.569	-11.845	-12.030	225.0	0.000	9.3E+05	0.0117	-0.998	-0.998	-13.028
243.8	-13.234	-0.668	-13.902	-14.111	243.8	0.000	1.0E+06	0.0115	-1.152	-1.152	-15.263
262.5	-15.348	-0.774	-16.123	-16.358	262.5	0.000	1.1E+06	0.0114	-1.324	-1.324	-17.683

Appendix A11: Tabulated head loss and static load for tunnel components as a function of flow rate.

Station 5 (plenum inlet)	A = Est. Cp =	1.556 0.57	ft^2 Cp,i =	0.84

V5 (ft/s)	Static Load (in. wg)	Friction Load (in. wg)	Total Head (in. wg)	P5 (in wg)
5.4	0.073	-0.021	0.051	-0.049
10.7	0.290	-0.085	0.205	-0.179
16.1	0.653	-0.192	0.461	-0.387
21.4	1.161	-0.341	0.820	-0.668
26.8	1.814	-0.533	1.281	-1.027
32.1	2.612	-0.768	1.844	-1.464
37.5	3.556	-1.045	2.510	-1.974
42.9	4.644	-1.365	3.279	-2.559
48.2	5.878	-1.728	4.150	-3.222
53.6	7.257	-2.133	5.123	-3.953
58.9	8.780	-2.581	6.199	-4.761
64.3	10.449	-3.072	7.377	-5.651
69.6	12.264	-3.605	8.658	-6.605
75.0	14.223	-4.181	10.041	-7.641

Station 6 (filter inlet)	A = Ke =	13.444 0.8	ft^2

V6 (ft/s)	Static Load (in. wg)	Friction Load (in. wg)	Total Head (in. wg)	P6 (in wg)
0.6	0.006	-0.005	0.001	-0.048
1.2	0.025	-0.021	0.005	-0.174
1.9	0.057	-0.046	0.011	-0.376
2.5	0.102	-0.083	0.019	-0.649
3.1	0.159	-0.129	0.030	-0.997
3.7	0.229	-0.186	0.043	-1.421
4.3	0.312	-0.253	0.059	-1.915
5.0	0.407	-0.330	0.077	-2.482
5.6	0.515	-0.418	0.097	-3.125
6.2	0.636	-0.516	0.120	-3.832
6.8	0.770	-0.624	0.146	-4.616
7.4	0.916	-0.743	0.173	-5.477
8.1	1.075	-0.872	0.203	-6.401
8.7	1.247	-1.011	0.236	-7.405

No Diffuser

Station 6 (filter inlet)	A = Ke =	13.444 0.98	ft^2

V6 (ft/s)	Static Load (in. wg)	Friction Load (in. wg)	Total Head (in. wg)	P6 (in wg)
0.6	0.079	-0.077	0.001	0.001
1.2	0.316	-0.310	0.006	0.006
1.9	0.710	-0.697	0.013	0.013
2.5	1.263	-1.239	0.024	0.024
3.1	1.973	-1.936	0.037	0.037
3.7	2.841	-2.788	0.054	0.054
4.3	3.868	-3.794	0.073	0.073
5.0	5.051	-4.956	0.096	0.096
5.6	6.393	-6.272	0.121	0.121
6.2	7.893	-7.744	0.149	0.149
6.8	9.550	-9.370	0.181	0.181
7.4	11.366	-11.151	0.215	0.215
8.1	13.339	-13.087	0.252	0.252
8.7	15.470	-15.177	0.293	0.293

Appendix A11: Tabulated head loss and static load for tunnel components as a function of flow rate.

Station 7 (honeycomb inlet) 2 filters		A =	13.444	ft^2		Station 8 (fan inlet)		A =	3.142	ft^2	
		K =	36.19001219					K =	0.4	ft^2	
V7 (ft/s)	Filter Loss (in. wg)	Static Load (in. wg)	Friction Load (in. wg)	Total Head (in. wg)	P7 (in wg)	V8 (ft/s)	Static Load (in. wg)	Friction Geo (in. wg)	Friction HC (in. wg)	Total Head (in. wg)	P8 (in wg)
0.6	-0.006	0.000	-0.006	-0.006	-0.054	2.7	-0.001	-0.001	-0.010	-0.012	-0.066
1.2	-0.025	0.000	-0.025	-0.025	-0.199	5.3	-0.006	-0.003	-0.020	-0.028	-0.227
1.9	-0.056	0.000	-0.056	-0.056	-0.432	8.0	-0.013	-0.006	-0.029	-0.048	-0.480
2.5	-0.100	0.000	-0.100	-0.100	-0.749	10.6	-0.024	-0.010	-0.039	-0.073	-0.822
3.1	-0.156	0.000	-0.156	-0.156	-1.153	13.3	-0.037	-0.016	-0.049	-0.102	-1.255
3.7	-0.225	0.000	-0.225	-0.225	-1.646	15.9	-0.054	-0.023	-0.059	-0.135	-1.781
4.3	-0.306	0.000	-0.306	-0.306	-2.221	18.6	-0.073	-0.031	-0.068	-0.173	-2.394
5.0	-0.400	0.000	-0.400	-0.400	-2.882	21.2	-0.096	-0.040	-0.078	-0.214	-3.097
5.6	-0.506	0.000	-0.506	-0.506	-3.631	23.9	-0.121	-0.051	-0.088	-0.260	-3.891
6.2	-0.625	0.000	-0.625	-0.625	-4.457	26.5	-0.150	-0.063	-0.098	-0.310	-4.768
6.8	-0.756	0.000	-0.756	-0.756	-5.372	29.2	-0.181	-0.077	-0.107	-0.365	-5.737
7.4	-0.900	0.000	-0.900	-0.900	-6.377	31.8	-0.215	-0.091	-0.117	-0.424	-6.801
8.1	-1.056	0.000	-1.056	-1.056	-7.458	34.5	-0.253	-0.107	-0.127	-0.487	-7.944
8.7	-1.225	0.000	-1.225	-1.225	-8.630	37.1	-0.293	-0.124	-0.137	-0.554	-9.184

Station 7 (honeycomb inlet) 2 filters		A =	13.444	ft^2		Station 8 (fan inlet)		A =	3.142	ft^2	
		K =	36.19001219					K =	0.4	ft^2	
V7 (ft/s)	Filter Loss (in. wg)	Static Load (in. wg)	Friction Load (in. wg)	Total Head (in. wg)	P7 (in wg)	V8 (ft/s)	Static Load (in. wg)	Friction Geo (in. wg)	Friction HC (in. wg)	Total Head (in. wg)	P8 (in wg)
0.6	-0.006	0.000	-0.006	-0.006	-0.005	2.7	-0.001	-0.001	-0.010	-0.012	-0.017
1.2	-0.025	0.000	-0.025	-0.025	-0.019	5.3	-0.006	-0.003	-0.020	-0.028	-0.047
1.9	-0.056	0.000	-0.056	-0.056	-0.043	8.0	-0.013	-0.006	-0.029	-0.048	-0.091
2.5	-0.100	0.000	-0.100	-0.100	-0.076	10.6	-0.024	-0.010	-0.039	-0.073	-0.149
3.1	-0.156	0.000	-0.156	-0.156	-0.119	13.3	-0.037	-0.016	-0.049	-0.102	-0.221
3.7	-0.225	0.000	-0.225	-0.225	-0.171	15.9	-0.054	-0.023	-0.059	-0.135	-0.306
4.3	-0.306	0.000	-0.306	-0.306	-0.233	18.6	-0.073	-0.031	-0.068	-0.173	-0.406
5.0	-0.400	0.000	-0.400	-0.400	-0.304	21.2	-0.096	-0.040	-0.078	-0.214	-0.519
5.6	-0.506	0.000	-0.506	-0.506	-0.385	23.9	-0.121	-0.051	-0.088	-0.260	-0.645
6.2	-0.625	0.000	-0.625	-0.625	-0.476	26.5	-0.150	-0.063	-0.098	-0.310	-0.786
6.8	-0.756	0.000	-0.756	-0.756	-0.575	29.2	-0.181	-0.077	-0.107	-0.365	-0.940
7.4	-0.900	0.000	-0.900	-0.900	-0.685	31.8	-0.215	-0.091	-0.117	-0.424	-1.108
8.1	-1.056	0.000	-1.056	-1.056	-0.804	34.5	-0.253	-0.107	-0.127	-0.487	-1.290
8.7	-1.225	0.000	-1.225	-1.225	-0.932	37.1	-0.293	-0.124	-0.137	-0.554	-1.486

Appendix A11: Tabulated head loss and static load for tunnel components as a function of flow rate.

Dissipated Total Friction Loss (in wg)	Conserved Total Static Load (in wg)	Check Theoretical Static load (in wg)	Total Pressure (in wg)		Test Section Velocity (ft/s)
-0.06	-0.002	-0.002	-0.066	0.066	18.8
-0.22	-0.006	-0.006	-0.227	0.227	37.5
-0.47	-0.014	-0.014	-0.480	0.480	56.3
-0.80	-0.025	-0.025	-0.822	0.822	75.0
-1.22	-0.040	-0.040	-1.255	1.255	93.8
-1.72	-0.057	-0.057	-1.781	1.781	112.5
-2.32	-0.077	-0.077	-2.394	2.394	131.3
-3.00	-0.101	-0.101	-3.097	3.097	150.0
-3.76	-0.128	-0.128	-3.891	3.891	168.8
-4.61	-0.158	-0.158	-4.768	4.768	187.5
-5.55	-0.191	-0.191	-5.737	5.737	206.3
-6.57	-0.228	-0.228	-6.801	6.801	225.0
-7.68	-0.267	-0.267	-7.944	7.944	243.8
-8.87	-0.310	-0.310	-9.184	9.184	262.5

Dissipated Total Friction Loss (in wg)	Conserved Total Static Load (in wg)	Check Theoretical Static load (in wg)	Total Pressure (in wg)		Test Section Velocity (ft/s)
-0.12	-0.002	-0.002	-0.117	0.117	18.8
-0.42	-0.006	-0.006	-0.431	0.431	37.5
-0.92	-0.014	-0.014	-0.939	0.939	56.3
-1.61	-0.025	-0.025	-1.637	1.637	75.0
-2.49	-0.040	-0.040	-2.528	2.528	93.8
-3.56	-0.057	-0.057	-3.615	3.615	112.5
-4.81	-0.077	-0.077	-4.890	4.890	131.3
-6.26	-0.101	-0.101	-6.357	6.357	150.0
-7.89	-0.128	-0.128	-8.017	8.017	168.8
-9.70	-0.158	-0.158	-9.862	9.862	187.5
-11.71	-0.191	-0.191	-11.901	11.901	206.3
-13.91	-0.228	-0.228	-14.137	14.137	225.0
-16.29	-0.267	-0.267	-16.553	16.553	243.8
-18.86	-0.310	-0.310	-19.169	19.169	262.5

Appendix A11: Tabulated head loss and static load for tunnel components as a function of flow rate.

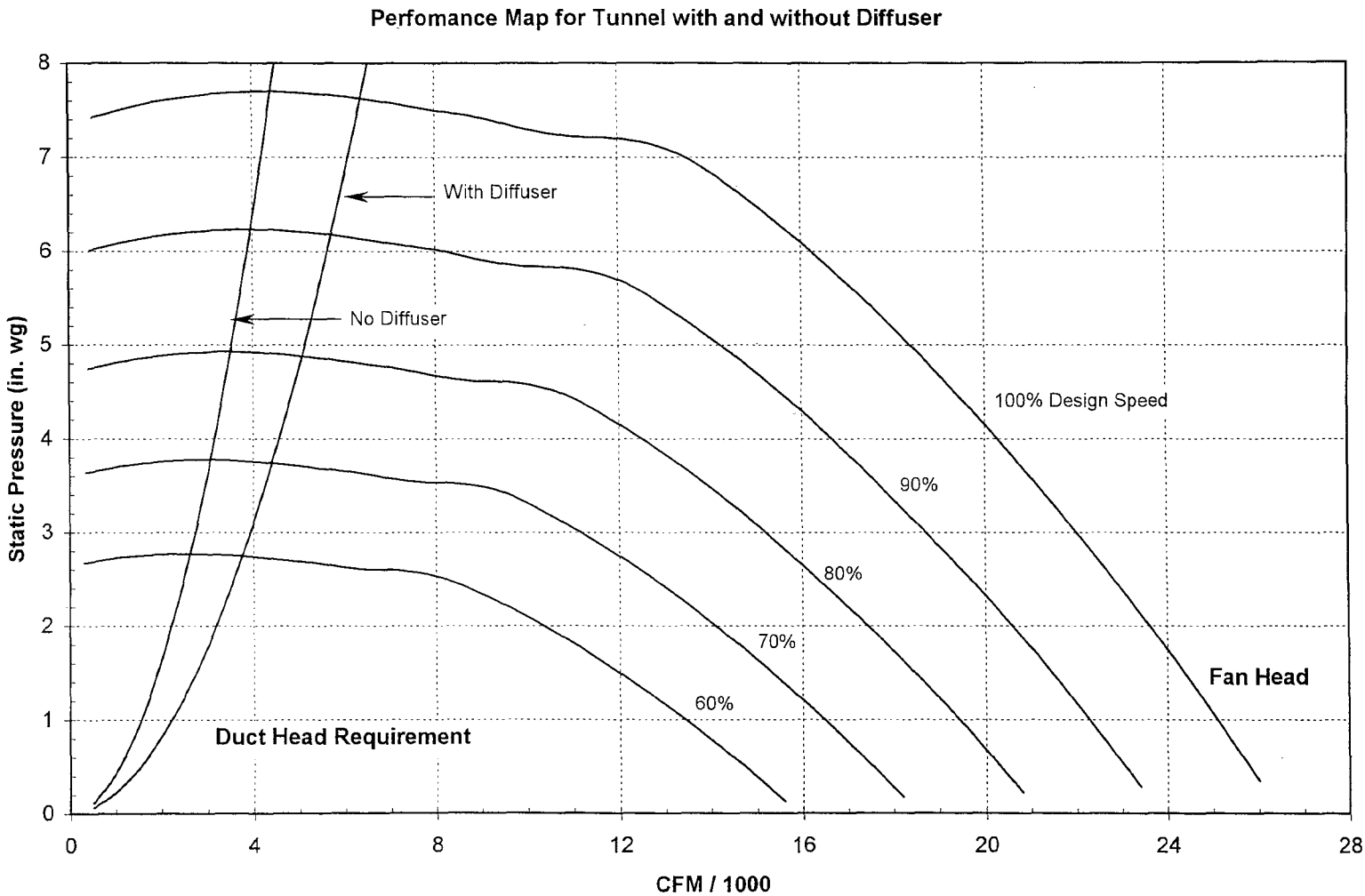

Appendix A12: Scaled fan performance with corresponding head requirement for tunnel duct system both with and without diffuser.

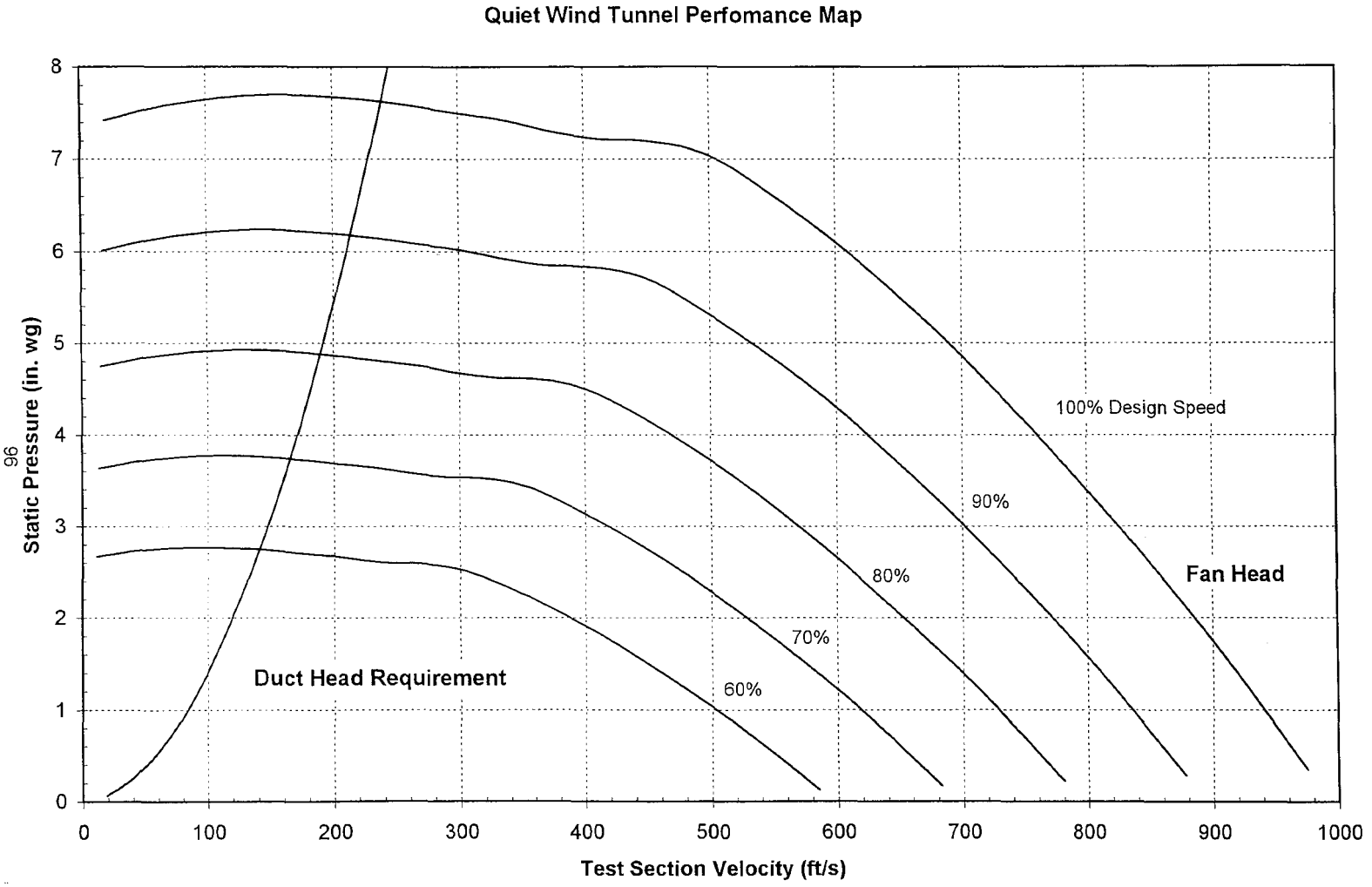

Appendix A13: Quiet wind tunnel performance characteristics as a function of test section velocity.

Tufcote Polyether Urethane Foam Typical Properties

Property	Test Method	E-50SM	E-75SM	E-100SM	E-200SM	E-100CM
Physical Properties						
Top Surface		1 mil Aluminized Polyester				1 mil Clear Polyester
Thickness		0.50	0.75	1.0	2.0	1.0
Density Nominal (lb./ft.³)	ASTM D3574	2.0	2.0	2.0	2.0	2.0
Weight Nominal (lb./ft.²)	ASTM D3574	.08	.13	.17	.35	.17
Flame	UL 94H	Meets HBF	Meets HBF	Meets HBF	Meets HBF	Meets HBF
	MVSS 302	Passes	Passes	Passes	Passes	Passes
	FAR 25.853 (b)					
	SAE J369 (a)					
Random Incidence Acoustical Absorption Coefficient	ASTM C423-84a and ASTM E795-83 (Mounting A) @ 125 Hz	0.11	0.12	0.20	0.50	0.17
	@ 250 Hz	0.08	0.30	0.81	0.82	0.74
	@ 500 Hz	0.60	0.67	0.61	0.91	0.63
	@1000 Hz	0.67	0.81	0.73	0.86	0.78
	@2000 Hz	0.87	0.77	0.71	0.75	0.69
	@4000 Hz	0.73	0.78	0.69	0.73	0.73
	NRC	0.55	0.65	0.70	0.80	0.70
Thermal Conductivity (K) (BTU-in./hr.-ft.²-deg.F)	ASTM C177			0.28		0.28
Thermal Resistivity (R) (hr.-ft.²-deg.F/BTU)	ASTM C177 *Calculated from 1-in. foam value	1.8*	2.7*	3.8	7.1*	3.8
Strength Properties						
Tensile Strength	ASTM D3574 Foam: lb. @ 23°C, ambient humidity			19		19
	Foam: lb. @ 70°C, 100% humidity x 2 wk.			18		18
	Foam: lb. @ 100°C, 100% humidity x 2 wk.			15		15
	Facing: lb.	36	36	36	36	17
Tear Strength	ASTM D3574 Foam: lb./in.			3.0		3.0
	Facing: lb./in. @ 1-in. width	0.6	0.6	0.6	0.6	0.7
Elongation* *Foam only	ASTM D3574 % @ room temp., ambient humidity			286		286
	% @ 70°C, 100% humidity x 2 wk.			350		350
	% @ 100°C, 100% humidity x 2 wk.			282		282
Compression Set	ASTM D3574 (% of original height @ 50% initial deflection, 70°C for 22 hr.)			18		18
Compression-Deflection	ASTM D3574, @ 50% Compression @ room temp., ambient humidity, psi			0.52		0.53
	@ 70°C, 100% humidity x 2 wk., psi			0.65		0.67
	@ 100°C, 100% humidity x 2 wk., psi			0.68		0.87

Appendix A14: Physical properties of acoustic foam provided by EAR Specialty Composites. Foam E-200 SM was selected to be sued as a wall lining on the tunnel ducts.

VITA

Christopher John Vincent was born October 19, 1976 in Easton, Pennsylvania. He is the son of John Anthony Vincent and Patricia Ann Vincent. He graduated from Lehigh University in January 2001 with a High Honors Bachelor of Science Degree in Mechanical Engineering. Upon graduation, he was awarded a full tuition grant and teaching assistantship for the pursuit of graduate studies in Mechanical Engineering at Lehigh University. He attended the University full-time until May 2002 when he accepted a position with the Integrated Defense Systems business unit of Boeing in Philadelphia, Pennsylvania.

END OF TITLE